European Journal of Medicinal Chemistry 150 (2018) 366–384

Contents lists available at ScienceDirect

European Journal of Medicinal Chemistry

journal homepage: http://www.elsevier.com/locate/ejmech

Research paper

Discovery of 4-((*N*-(2-(dimethylamino)ethyl)acrylamido)methyl)-*N*-(4-methyl-3-((4-(pyridin-3-yl)pyrimidin-2-yl)amino)phenyl) benzamide (CHMFL-PDGFR-159) as a highly selective type II PDGFRα kinase inhibitor for PDGFRα driving chronic eosinophilic leukemia

Qiang Wang [a, b, 1], Feiyang Liu [a, c, 1], Shuang Qi [a, b, 1], Ziping Qi [a, b, 1], Xiao-E. Yan [d, 1], Beilei Wang [a, c], Aoli Wang [a, c], Wei Wang [a, b], Cheng Chen [a, c], Xiaochuan Liu [a, b], Zongru Jiang [a, c], Zhenquan Hu [a, b], Li Wang [a, c], Wenchao Wang [a, b], Tao Ren [e], Shanchun Zhang [b, f], Cai-Hong Yun [d, *], Qingsong Liu [a, b, c, e, g, **], Jing Liu [a, b, g, ***]

[a] *High Magnetic Field Laboratory, Chinese Academy of Sciences, Mailbox 1110, 350 Shushanhu Road, Hefei, Anhui, 230031, PR China*
[b] *CHMFL-HCMTC Target Therapy Joint Laboratory, 350 Shushanhu Road, Hefei, Anhui, 230031, PR China*
[c] *University of Science and Technology of China, Hefei, Anhui, 230036, PR China*
[d] *Institute of Systems Biomedicine, Department of Biophysics, School of Basic Medical Sciences, Peking University Health Science Center, Beijing, 100191, PR China*
[e] *Precision Targeted Therapy Discovery Center, Institute of Technology Innovation, Hefei Institutes of Physical Science, Chinese Academy of Sciences, Hefei, Anhui, 230088, PR China*
[f] *Hefei Cosource Medicine Technology Co. LTD., 358 Ganquan Road, Hefei, Anhui, 230031, PR China*
[g] *Hefei Science Center, Chinese Academy of Sciences, 350 Shushanhu Road, Hefei, 230031, Anhui, PR China*

ARTICLE INFO

Article history:
Received 18 September 2017
Received in revised form
12 February 2018
Accepted 1 March 2018
Available online 20 March 2018

Keywords:
PDGFR kinase
Type II inhibitor
Kinase inhibitor
CEL

ABSTRACT

Through exploration of the non-highly conserved allosteric hydrophobic pocket generated by DFG-out shifting in the inactive conformation, we discovered a highly selective type II PDGFRα kinase inhibitor **15i** (CHMFL-PDGFRα-159), which exhibited strong potency against purified PDGFRα (IC_{50}: 132 nM) but not structurally similar PDGFRβ, ABL, c-KIT and VEGFR2 kinases. In addition, it displayed a high selectivity profile (S score (10) = 0.02) at the concentration of 1 μM among 468 kinases/mutants in the KINOMEscan profiling. X-ray crystal structure of **15i** in complex with PDGFRα revealed a distinct binding feature in the allosteric hydrophobic pocket which might help to expand the diversity of type II kinase inhibitors. Compound **15i** potently inhibited the proliferation of PDGFRα driving Chronic Eosinophilic Leukemia (CEL) cell line EOL-1 through strong blockage of PDGFRα mediated signaling pathways, arresting cell cycle progression, and induction of apoptosis. Furthermore, compound **15i** effectively suppressed the EOL-1 tumor progression in the xenograft model and increased the survival rate in the engraftment tumor model.

Abbreviations used: PDGFR, platelet-derived growth factor receptor; RTK, Receptor Tyrosine Kinases; ABL kinase, Abelson kinase; KIT kinase, v-kit Hardy-Zuckerman 4 feline sarcoma viral oncogene homolog; RTK, receptor tyrosine kinase; CEL, Chronic Eosinophilic Leukemia; GISTs, Gastrointestinal Stromal Tumors; SAR, structure-activity relationship; NSCLC, non-small cell lung cancer; STAT3, signal transducer and activator of transcription 3; ERK, extracellular regulated protein kinases; PARP, poly ADP-ribose polymerase; PK, pharmacokinetics; PD, Pharmacodynamics; IHC, immunohistochemistry; HE, hematoxylin-eosin; TUNEL, terminal deoxynucleotidyl transferase dUTP nick end labeling; TGI, tumor growth inhibition; IP, intraperitoneal injection.

* Corresponding author. Institute of Systems Biomedicine, Department of Biophysics, School of Basic Medical Sciences, Peking University Health Science Center, Beijing, 100191, PR China.
** Corresponding author. High Magnetic Field Laboratory, Chinese Academy of Sciences, Mailbox 1110, 350 Shushanhu Road, Hefei, Anhui, 230031, PR China.
*** Corresponding author. High Magnetic Field Laboratory, Chinese Academy of Sciences, Mailbox 1110, 350 Shushanhu Road, Hefei, Anhui, 230031, PR China.
E-mail addresses: yunch@hsc.pku.edu.cn (C.-H. Yun), qsliu97@hmfl.ac.cn (Q. Liu), jingliu@hmfl.ac.cn (J. Liu).
[1] These authors contribute equally.

https://doi.org/10.1016/j.ejmech.2018.03.003
0223-5234/

1. Introduction

Platelet-derived growth factor receptors (PDGFRs), including PDGFRα and PDGFRβ, are class III receptor tyrosine kinases (RTK) that can be activated by PDGFs and play important roles in the basic physiological functions, such as organogenesis and angiogenesis [1–3]. Dysregulation of PDGFRs, especially PDGFRα, has been observed in a variety of human tumors including sarcomas, gastrointestinal stromal tumors (GISTs), glioblastomas and chronic eosinophilic leukemia (CEL) etc. [4–6] Due to the critical role of PDGFRα in tumorigenesis, it has been extensively explored as a drug discovery target. To date, a number of kinase inhibitors have been reported to bear PDGFRs activities, such as compounds **1** (Imatinib) [7,8], **2** (Sunitinib) [9], **3** (Ponatinib) [10], **4** (Axitinib) [11], **5** (Masitinib) [12], **6** (Crenolanib) [13], **7** (Nintedanib) [14], **8** (Linfanib) [15,16] and **9** (Amuvatinib) [16] (Fig. 1). However, all of these inhibitors are multiple-target compounds and highly selective PDGFRα inhibitor is in urgent need both for fundamental research and clinical application.

Besides PDGFRs, class III RTK family also includes c-KIT, FLT3 and CSF1R [17]. Structurally, class III RTKs are comprised by five extracellular immunoglobulin-like repeats and a kinase insert separating the ATP-binding and phosphotransferase regions of the kinase domain. The ATP-binding pockets of type III RTK family are highly conserved, which makes it quite challenging to develop selective inhibitors. Type II inhibitors that bind to the inactive (DFG out) conformation of the kinase, sometimes can take advantage of the additional DFG-shift generated allosteric pocket to achieve higher selectivity [18]. Given this fact, we postulated that modification of the DFG region-binding moiety of the suitable pharmacophore might lead to more selective inhibitors. Inspired by this assumption and via the structure-guided drug design approach, starting from the known BCR-ABL/cKIT inhibitor imatinib that also bears PDGFR activity, we discovered a highly selective type II PDGFRα inhibitor **15i** (CHMFL-PDGFRα-159) (Fig. 2).

2. Results and discussion

2.1. Chemistry and structure-activity relationship (SAR) investigation

As depicted in Scheme 1, compounds **13a-n** were prepared starting from amidation reaction between 6-methyl-*N*-(4-(pyridin-3-yl)pyrimidin-2-yl)benzene-1,3-diamine (**10**) and corresponding substituted benzoyl chloride or benzoic acid derivatives to form intermediates **11a-f**. Then, compounds **11a-b** were treated with NaN_3 and subsequently the azido groups were hydrogenated to yield the amine intermediates **12a-b**. Compound **12c** was generated by deprotection of the Boc group under acidic condition from **11c**. For the synthesis of compounds **12d-f**, the nitro groups in **11d-f** were hydrogenated to afford the amine products directly. Finally, amidation reaction between amine analogs **12a-f** and R4-substituted acyl chloride derivatives furnished the target compounds **13a-n**. Compounds **15a-r** were prepared beginning with nucleophilic substitution reaction of intermediate **11a** with different substituted amines to give intermediates **14a-e**. Then amidation reaction between amine analogs **14a-e** and a panel of R5-substituted acyl chloride derivatives afforded the products **15a-r**.

For SAR exploration, we used IL3 independent BaF3 cells expressing the fusion kinases TEL-PDGFRα, TEL-PDGFRβ, TEL-c-KIT and TEL-VEGFR2 as the primary readout of the activity and selectivity of the compounds. Ideally in this assay the highly selective

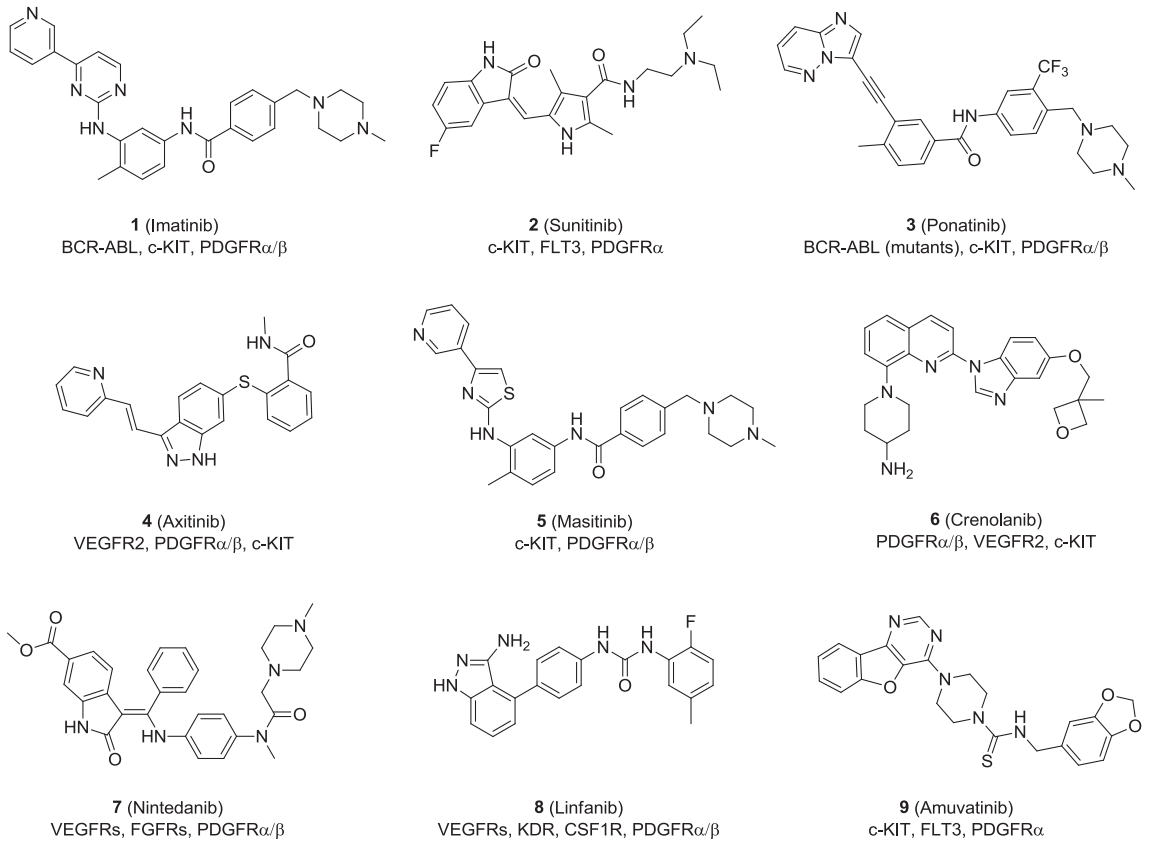

Fig. 1. Representative multi-target kinase inhibitors with PDGFRs activity.

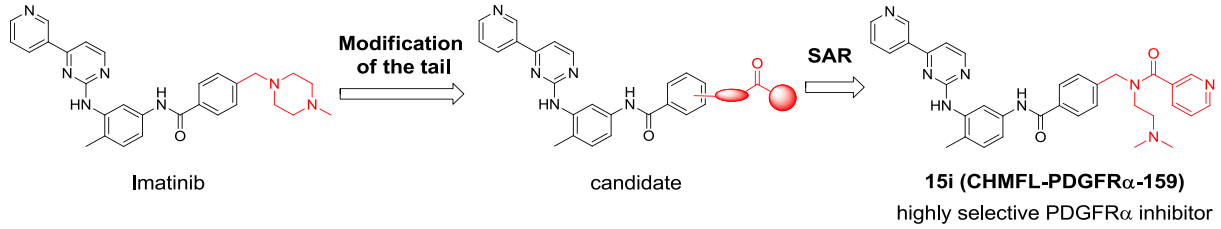

Fig. 2. Schematic illustration of the discovery of PDGFRα selective inhibitor **15i**.

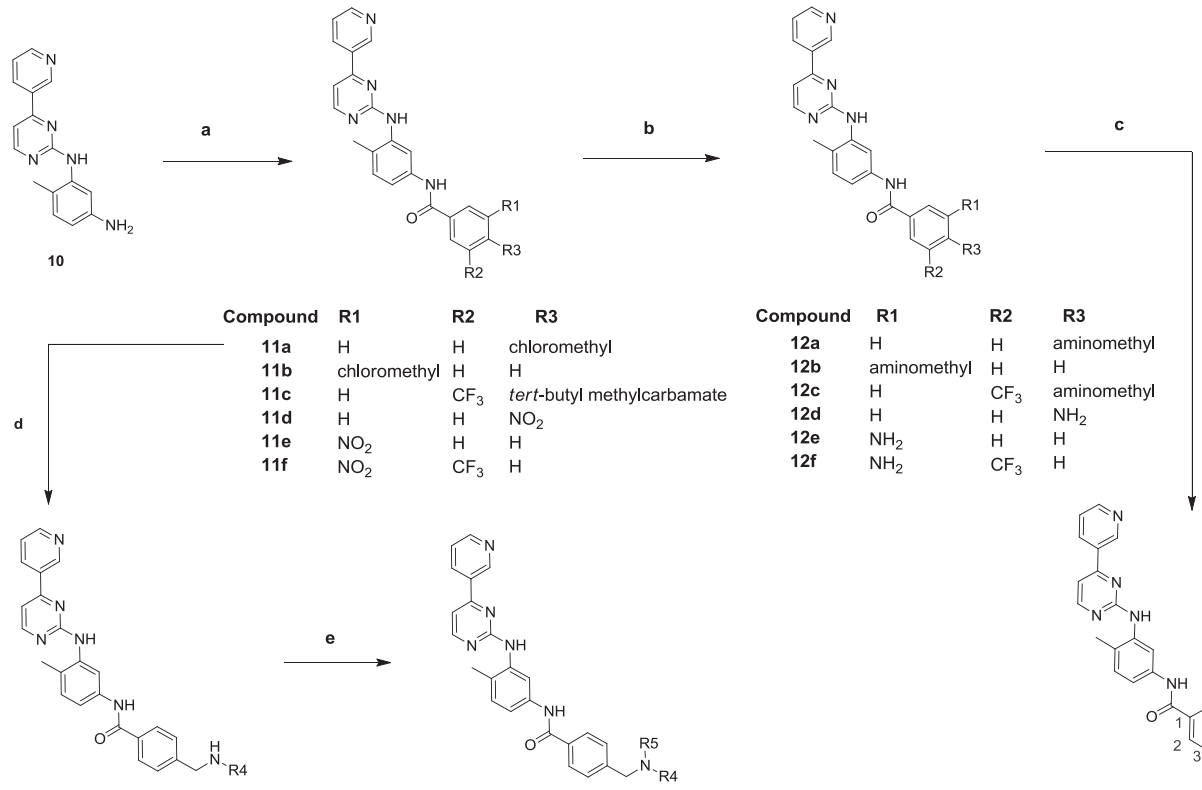

Compound	R1	R2	R3
11a	H	H	chloromethyl
11b	chloromethyl	H	H
11c	H	CF_3	*tert*-butyl methylcarbamate
11d	H	H	NO_2
11e	NO_2	H	H
11f	NO_2	CF_3	H

Compound	R1	R2	R3
12a	H	H	aminomethyl
12b	aminomethyl	H	H
12c	H	CF_3	aminomethyl
12d	H	H	NH_2
12e	NH_2	H	H
12f	NH_2	CF_3	H

Compound	R4
14a	*N*,*N*-dimethylethanamine
14b	isopentane
14c	triethylamine
14d	1-ethylpyrrolidine
14e	ethanol

Compound	R4	R5
15a	*N*,*N*-dimethylethanamine	-acryloyl
15b	*N*,*N*-dimethylethanamine	-propionyl
15c	*N*,*N*-dimethylethanamine	-(*E*)-but-2-enoyl
15d	*N*,*N*-dimethylethanamine	-cyclopropanecarbonyl
15e	*N*,*N*-dimethylethanamine	-isobutyryl
15f	*N*,*N*-dimethylethanamine	-n-butyryl
15g	*N*,*N*-dimethylethanamine	-pivaloyl
15h	*N*,*N*-dimethylethanamine	-2-(dimethylamino)acetyl
15i	*N*,*N*-dimethylethanamine	-nicotinoyl
15j	*N*,*N*-dimethylethanamine	-isoxazole-5-carbonyl
15k	*N*,*N*-dimethylethanamine	-thiophene-2-carbonyl
15l	*N*,*N*-dimethylethanamine	4-methylbenzoyl
15m	triethylamine	-acryloyl
15n	triethylamine	-nicotinoyl
15o	1-ethylpyrrolidine	-nicotinoyl
15p	isopentane	-propionyl
15q	ethanol	-nicotinoyl
15r	ethanol	-2-(dimethylamino)acetyl

Compound	n	R2	-$(CH_2)_n$NH-R4 Substitution Position	R4
13a	1	H	4	-propionyl
13b	1	H	4	-acryloyl
13c	1	H	4	-ethenesulfonyl
13d	1	H	4	-nicotinoyl
13e	1	H	5	-propionyl
13f	1	H	5	-acryloyl
13g	1	CF_3	4	-acryloyl
13h	1	CF_3	4	-nicotinoyl
13i	0	H	4	-propionyl
13j	0	H	4	-acryloyl
13k	0	H	4	-nicotinoyl
13l	0	H	5	-acryloyl
13m	0	CF_3	5	-acryloyl
13n	0	CF_3	5	-propionyl

Scheme 1. Synthesis of Compounds 13a-n and 15a-r[a].

[a]Reagents and conditions: (a) for **11a-b**: 4- or 3-(chloromethyl)benzoyl chloride, DMF, Et_3N, 0 °C, 2 h; for **11c-f**: corresponding substituted benzoic acid derivatives, HATU, DIPEA, DMF, rt, 2 h; (b) for **12a-b**: i) NaN_3, DMF, rt, overnight; ii) H_2, Pd/C, EtOAc, rt, 6 h; for **12c**: 4 N HCl in EtOAc, rt, 6 h; for **12d-f**: H_2, Pd/C, EtOAc, rt, 6 h; (c) R4-COCl, DMF, Et_3N, 0 °C, 2 h; (d) R4-NH_2, DMF, rt, overnight; (e) R5-COCl, DMF, Et_3N, 0 °C, 2 h.

and potent compound would show strong anti-proliferation efficacy against TEL-PDGFRα-BaF3 rather than BaF3 cells. As shown in the general structure, we first modified the allosteric binding region of imatinib (Table 1). When R2 was H and the CH_2NHR_4

Table 1
SAR exploration focused on the R2/R4 Moieties.[a]

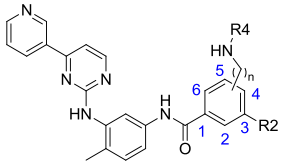

Compd	(CH_2)nNH-R4 *Position*/ n = 0 or 1	R2	R4	Parental BaF3 (GI_{50}:μM)	TEL-PDGFRα BaF3 (GI_{50}:μM)	TEL-PDGFRβ BaF3 (GI_{50}:μM)	TEL-VEGFR2 BaF3 (GI_{50}:μM)	TEL-c-KIT BaF3 (GI_{50}:μM)
1	–	–	–	>10	0.034 ± 0.008	0.019 ± 0.004	>10	0.37 ± 0.067
13a	*Position*-4 n = 1	H		>10	0.014 ± 0.002 *P* = 0.0001	0.201 ± 0.058 *P* = 0.0001	>10	6.22 ± 0.18 *P* = 0.0001
13b	*Position*-4 n = 1	H		>10	0.034 ± 0.003 *P* = 0.0001	0.155 ± 0.013 *P* = 0.0001	>10	>10
13c	*Position*-4 n = 1	H		7.71 ± 0.12	0.013 ± 0.007 *P* = 0.0001	0.048 ± 0.024 *P* = 0.5659	1.56 ± 0.312	0.58 ± 0.036 *P* = 0.8486
13d	*Position*-4 n = 1	H		1.12 ± 0.068	0.014 ± 0.001 *P* = 0.0001	0.341 ± 0.067	0.348 ± 0.052	0.216 ± 0.015 *P* = 0.0001
13e	*Position*-5 n = 1	H		4.75 ± 0.054	0.015 ± 0.002 *P* = 0.0001	0.221 ± 0.042	3.22 ± 0.19	2.92 ± 0.069 *P* = 0.0001
13f	*Position*-5 n = 1	H		>10	0.16 ± 0.002 *P* = 0.0001	0.244 ± 0.009	>10	4.75 ± 0.61 *P* = 0.0001
13g	*Position*-4 n = 1	CF_3		>10	0.059 ± 0.001 *P* = 0.0001	0.161 ± 0.082	>10	0.30 ± 0.002 *P* = 0.0001
13h	*Position*-4 n = 1	CF_3		8.33 ± 0.089	0.005 ± 0.001 *P* = 0.0001	0.082 ± 0.013	3.41 ± 0.12	0.066 ± 0.004 *P* = 0.0001
13i	*Position*-4 n = 0	H		>10	0.012 ± 0.002 *P* = 0.0001	0.888 ± 0.064	6.27 ± 0.34	4.94 ± 0.088 *P* = 0.0001
13j	*Position*-4 n = 0	H		5.60 ± 0.054	0.044 ± 0.002 *P* = 0.0036	0.757 ± 0.044	2.03 ± 0.71	2.94 ± 0.067 *P* = 0.0001
13k	*Position*-4 n = 0	H		1.70 ± 0.044	0.013 ± 0.004 *P* = 0.0001	0.583 ± 0.016	0.882 ± 0.069	0.426 ± 0.005 *P* = 0.0001
13l	*Position*-5 n = 0	H		2.48 ± 0.031	0.008 ± 0.001 *P* = 0.0001	0.173 ± 0.017	1.57 ± 0.15	1.53 ± 0.068 *P* = 0.0001
13m	*Position*-5 n = 0	CF_3		5.46 ± 0.13	0.013 ± 0.005 *P* = 0.0001	0.098 ± 0.001 *P* = 0.0488	3.34 ± 0.02	0.25 ± 0.021 *P* = 0.1517
13n	*Position*-5 n = 0	CF_3		>10	0.039 ± 0.008 *P* = 0.0001	0.231 ± 0.001	>10	0.104 ± 0.023 *P* = 0.0001

[a] All GI_{50} values (mean ± SD) were obtained by triplet testing and calculated using Prism 5.0 (GraphPad Software, San Diego, CA) by linear regression analysis. *p*-Value calculation: Using one-way ANOVA (and nonparametric) method of column analyses in Prism 5.0 (GraphPad Software, San Diego, CA), the p-values were calculated by using imatinib as the reference compound.

substitutes were fixed at the 4-position of the benzene ring, a series of R4 groups, *i.e.*, propionyl (**13a**), acryloyl (**13b**), ethenesulfonyl (**13c**) and nicotinoyl (**13d**), were examined. As displayed in Table 1, both compound **13a** and **13b** presented good inhibitory activity against PDGFRα, with moderate selectivity against PDGFRβ and high selectivity over VEGFR2, c-KIT dependent BaF3 cells. Meanwhile, these two compounds did not affect parental BaF3 cell line. These results suggested that the modification of the 4-position of the benzene ring might be reasonable for obtaining the PDGFRα selectivity. Compound **13c**, which has a similar ethenesulfonyl moiety to **13b**'s acryloyl moiety, gave comparable activity against PDGFRα with **13b** and **13a**. But it also exhibited activities against PDGFRβ, VEGFR2 and c-KIT kinases, indicating that the sulfonyl group was unfavorable for obtaining the PDGFRα selectivity. Compound **13d**, which has a bigger nicotinoyl moiety at the 4-position of the phenyl ring, showed comparable PDGFRα/β activities with **13b** but improved selectivity. However, it also inhibited VEGFR2, c-KIT and parental BaF3 cells. Simply shifting the -CH_2NHR4 substituent from the 4- to 5-position of the benzene ring (**13e**-**f**) did not lead to better selectivity, which suggested that the modification of the 5-position of the benzene ring might be unfavorable for acquiring the PDGFRα selectivity. When the H atom was replaced by a more hydrophobic CF_3 group at R2 (**13g**-**h**), compound **13g** presented comparable potency profile with **13b** but increased c-KIT activity. Compound **13h** showed stronger activities against PDGFRα/β and c-KIT than **13d**, however its selectivity profile was undesirable. When the -NHR4 substituent was introduced to the 4-position of the benzene ring and R2 was kept as the H atom

(**13i-k**), compounds **13i-j** achieved good selectivity between PDGFRα/β but also exhibited moderate activities against VEGFR2 and c-KIT. The potency and selectivity profile of **13k** was similar to **13d**. Simply shifting the -NHR4 substituent from the 4- to 5-position of the benzene ring (**13l)** provided no better results. When the H atom was replaced by a CF_3 group at R2 (**13m-n**), the selectivity for PDGFRα was greatly decreased. These results suggested that fixing the substituent at the 4-position of the benzene ring and keeping the H atom at R2 were preferred for PDGFRα activity and selectivity over other structurally similar kinases.

In order to achieve better selectivity between PDGFRα and PDGFRβ, we further explored the SAR of the R4/R5 moieties (Table 2). When R5 was *N*,*N*-dimethylethylene and R4 was acrylamide (**15a**), high potency against PDGFRα (GI_{50}: 0.011 μM) and more than 30-fold selectivity over PDGFRβ were obtained. Meanwhile, no apparent activities against VEGFR2, c-KIT and parental BaF3 cells were observed. Saturation of the acrylamide to propionyl at R4 (**15b**) also achieved about 14-fold selectivity over PDGFRβ although the potency against PDGFRα was slighted decreased. In addition, compound **15b** did not inhibit VEGFR2, c-KIT or parental BaF3 cells like **15a**, which indicated that the *N*,*N*-dimethylethanamine group on the amide NH of **13a/13b** indeed favored the PDGFRα selectivity. Based on these positive results, a series of R4 groups were examined. Increasing the size of R4 (**15c-g)** led to no better selectivity between PDGFRα and PDGFRβ, meanwhile similar potencies against PDGFRα were retained compared with **15a**. Compound **15h**, which has a 2-(dimethylamino)acetyl group at R4, gave better selectivity but lost about 10-fold potency against PDGFRα compared with **15a** (GI_{50}: 0.12 μM versus 0.011 μM). When changing the substitute at R4 to the nicotinoyl group (**15i)**, it exhibited about 85-fold selectivity between PDGFRα and PDGFRβ, meanwhile retained good activity against PDGFRα (GI_{50}: 0.034 μM). Other aromatic acyl moieties at R4 position (**15j-l**) all resulted in selectivity loss between PDGFRα and PDGFRβ. These results suggested that the nicotinoyl group might help to provide a preferable binding mode to PDGFRα. When R4 was H atom (**14a**), the high potency against PDGFRα was retained but the selectivity over other kinases was decreased in comparison with **15a** and **15i**, indicating that the acyl group was critical for the PDGFRα/β selectivity, although not all acyl groups favored the selectivity and activity (**15c-g** and **15j-l**). We then investigated a series of R5 groups, *i.e.*, triethylamine (**15m-n**), 1-ethylpyrrolidine (**15o**), isopentane (**15p)** and ethanol (**15q-r)** for SAR study but didn't obtain better selectivity than **15i**. Compounds **15m-n** displayed lower activity and selectivity compared with **15a** and **15i** respectively. Compound **15o** exhibited similar potency profile to **15i** with a 24-fold less selectivity between PDGFRα/β, while **15p** showed decreased selectivity to all the cell lines tested although the PDGFRα activity was retained. Both compounds **15q** and **15r** displayed much lower activity to PDGFRα, indicating that the ethanol moiety at R5 was unfavorable.

2.2. Biochemical and cellular property evaluation

Since compound **15i** exhibited the best selectivity and activity profile, we then chose it for further characterization. We first evaluated **15i**'s kinome-wide selectivity with DiscoveRx's KINOMEscan technology which could provide the relative binding activity of the compound against a panel of purified kinase proteins at a certain concentration [19]. The results showed that **15i** had high selectivity (S score (10) = 0.02) at the concentration of 1 μM against 468 kinases/mutants tested (Fig. 3A and Supplemental Table 1). Besides PDGFRα, **15i** also displayed strong binding to PDGFRβ, c-KIT, ABL1 and DDR1 kinases. Given the fact that KINOMEscan is a binding assay which may not truly reflect the inhibitory activity of the compound, we then employed ADP-Glo assay, which uses purified kinase protein to detect the compound's inhibitory activity for blocking the kinase's enzymatic function, for further validation of these potential targets (Fig. 3B). In the ADP-Glo assay, **15i** strongly inhibited PDGFRα with an IC_{50} of 132 nM and exhibited 46-fold selectivity over PDGFRβ (IC_{50}: 6115 nM). Meanwhile it showed no apparent inhibitory activity to ABL1 and c-KIT (both $IC_{50} > 10$ μM), and only exhibited weak inhibition to DDR1 kinase (IC_{50}: 2462 nM). These results further proved that **15i** was a highly selective PDGFRα inhibitor. Furthermore, we also tested **15i** against PDGFRα gatekeeper T674I mutant, which was reported to be resistant to imatinib [20]. Unfortunately, it did not exhibit potent anti-proliferative effect against BaF3 cells expressing TEL-PDGFRα-T674I mutant (GI_{50}: >10 μM) indicating that it could not overcome this gatekeeper mutant either.

In order to better understand the binding mode of compound **15i** to PDGFRα kinase, we obtained the co-crystal of **15i** in complex with PDGFRα (PDB ID: 5GRN, Supplemental Table 2). The complex structure was determined at high resolution (1.75 Å), which provided unambiguous information of how the compound bound to the kinase and provided insights into why this compound potently inhibits PDGFRα but not other structurally similar kinases such as ABL1, c-KIT and VEGFR2 etc. Compound **15i** bound to the canonical DFG-out inactive conformation of PDGFRα kinase in a typical type II binding mode (Fig. 4 A). The pyridine in the head moiety formed a hydrogen bond with Cys677 in the hinge binding area. The aminopyrimidine formed a hydrogen bond with the gatekeeper residue Thr674. The amide moiety connecting two benzene rings formed two signature hydrogen bonds with Glu644 in the c-helix and Asp836 in the DFG motif, respectively. The benzene ring adjacent to the carbonyl of this amide interacted with the side-chain of Met648 through hydrophobic interaction. Interestingly, the nicotinoyl group in R4 that occupied the hydrophobic pocket adopted a distinct distorted conformation that turned underneath the benzyl group to form an intramolecular π-π stacking interaction (Fig. 4B), which was rarely observed for type II kinase inhibitors. In addition, a water molecule bridged the *N*, *N*-dimethyl amine moiety (R5), Asp836, and His816, which further increased the binding affinity.

To explain the selectivity of compound **15i** against PDGFRα over other structurally similar kinases, we then docked **15i** into the known crystal structures of c-KIT (PDB ID: 4U0I), ABL1 (PDB ID: 2E2B), VEGFR2 (PDB ID: 3WZE), as well as PDGFRβ which was obtained by homology modeling (built from the PDGFRα X-ray crystal structure PDB ID: 5GRN). In the crystal structure of **15i** complexed with PDGFRα, the amide group of **15i** is partially stabilized by a weak hydrogen bond (3.5 Å) formed with Met648 residue located in the c-helix, while in c-KIT and VEGFR2 kinases this methionine residue is replaced by leucine that lacks the hydrogen bond formation capability. This may partially reduce the binding affinity of **15i** to c-KIT and VEGFR2 kinases. In addition, in the DFG-out shift formed hydrophobic pocket, **15i** forms a weak hydrogen bond (3.5 Å) with Cys814. However, in ABL1 kinase this Cys814 residue is replaced by a hydrophobic Phe359 residue, which might reduce the binding affinity of **15i** against ABL1 compared with PDGFRα kinase (Fig. 4C). In comparison with PDGFRα, PDGFRβ bears almost the same amino acids sequence in the drug binding pocket. However, there is only one different residue located in the hinge binding region. The nonpolar Phe678 in PDGFRα is replaced by the positively charged Arg684 in PDGFRβ (Fig. 4D). Although this residue is probably not involved in the direct binding to the drug, we suspect that there might be some factors that induce different protein conformation which could not be reflected by this homology computational study and required further detailed crystallography study.

We then examined **15i**'s antiproliferative effects on the PDGFRα

Table 2
SAR exploration focused on the R4/R5 Moieties.[a]

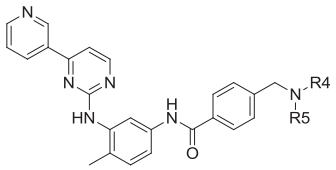

Compd	R4	R5	Parental BaF3 (GI_{50}:μM)	TEL-PDGFRα BaF3 (GI_{50}:μM)	TEL-PDGFRβ BaF3 (GI_{50}:μM)	TEL-VEGFR2 BaF3 (GI_{50}:μM)	TEL-c-KIT BaF3 (GI_{50}:μM)
14a	-H		>10	0.024 ± 0.011	0.125 ± 0.023	4.88 ± 0.21	5.0 ± 0.14
15a			>10	0.011 ± 0.04	0.35 ± 0.045	>10	>10
15b			>10	0.036 ± 0.02	0.504 ± 0.045	>10	>10
15c			>10	0.054 ± 0.008	0.219 ± 0.081	8.54 ± 0.41	>10
15d			>10	0.112 ± 0.094	0.437 ± 0.045	>10	>10
15e			>10	0.039 ± 0.094	0.123 ± 0.18	8.64 ± 0.22	6.11 ± 0.14 $P = 0.0001$
15f			>10	0.025 ± 0.001 $P = 0.0004$	0.09 ± 0.001	4.76 ± 0.61	5.75 ± 0.31 $P = 0.0001$
15g			>10	0.017 ± 0.007	0.061 ± 0.006	5.48 ± 0.059	2.53 ± 0.47 $P = 0.0001$
15h			>10	0.12 ± 0.018	9.2 ± 0.012	>10	>10
15i			>10	0.034 ± 0.005 $P = 0.0072$	2.9 ± 0.047 $P = 0.0001$	>10	>10
15j			>10	0.166 ± 0.33 $P = 0.0001$	0.787 ± 0.019 $P = 0.0001$	>10	>10
15k			>10	0.056 ± 0.26 $P = 0.0001$	0.207 ± 0.009 $P = 0.0001$	>10	>10
15l			>10	0.1 ± 0.29 $P = 0.0001$	0.24 ± 0.045 $P = 0.0001$	>10	>10
15m			5.45 ± 0.52	0.344 ± 0.021 $P = 0.0001$	1.10 ± 0.025 $P = 0.0001$	4.55 ± 0.064	5.14 ± 0.45 $P = 0.0001$
15n			>10	0.033 ± 0.003 $P = 0.9993$	0.699 ± 0.002 $P = 0.0001$	>10	>10
15o			>10	0.039 ± 0.007 $P = 0.3743$	0.934 ± 0.031 $P = 0.0001$	>10	>10
15p			5.62 ± 0.098	0.019 ± 0.008 $P = 0.0001$	0.23 ± 0.018 $P = 0.0001$	5.74 ± 0.81	3.94 ± 0.43 $P = 0.0001$
15q			>10	0.353 ± 0.046 $P = 0.0001$	3.02 ± 0.48 $P = 0.0001$	>10	>10
15r			>10	0.363 ± 0.093 $P = 0.0001$	3.88 ± 0.45 $P = 0.0001$	>10	>10

[a] All GI_{50} values (mean ± SD) were obtained by triplet testing and calculated using Prism 5.0 (GraphPad Software, San Diego, CA) by linear regression analysis. *p*-Value calculation: Using one-way ANOVA (and nonparametric) method of column analyses in Prism 5.0 (GraphPad Software, San Diego, CA), the p-values were calculated by using imatinib as the reference compound.

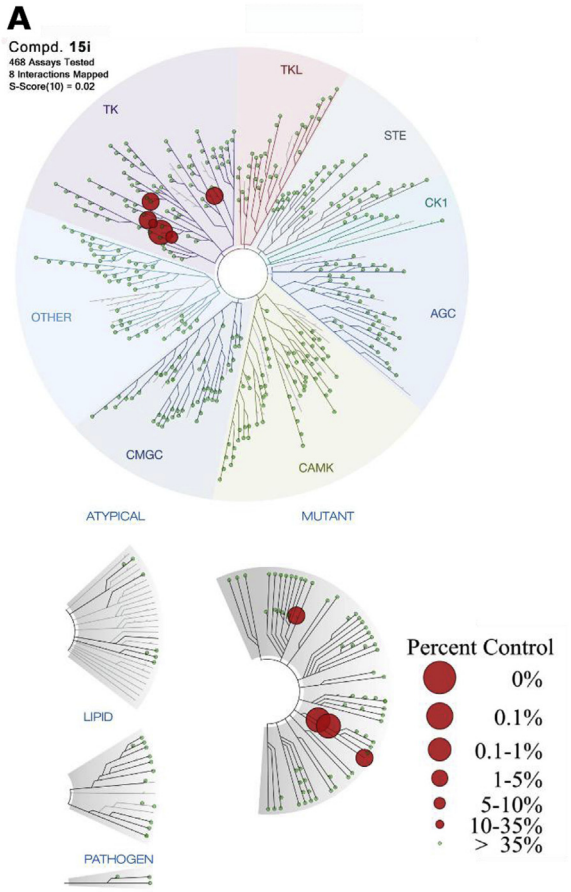

Kinase	Percent Control at 1 μM
PDGFRα	6.8
PDGFRβ	0.7
ABL1	4.9
DDR1	3.9
KIT	2.2

B

Kinase	15i IC_{50}/ nM
PDGFRα	132±10
PDGFRβ	6115±1498
ABL1	>10000
DDR1	2462±126
KIT	>10000

Fig. 3. Kinome wide selectivity profile of compound **15i**. (A) KINOMEscan profiling of **15i** at a concentration of 1 μM against 468 kinases: S score (10) = 0.02 at 1 μM. (B) Biochemical assay (Promega ADP-Glo) characterization of **15i**'s inhibitory activity against PDGFRα/β, ABL1, DDR1 and c-KIT kinases. All IC_{50} values were obtained by triple testing.

dependent/overexpressed cancer cell lines (Table 3). In the EOL-1 cell line, which are FIP1L1-PDGFRα-dependent chronic eosinophilic leukemia cells, both compounds **15i** and imatinib displayed strong antiproliferative efficacy (GI_{50}: <0.001 μM). In the non-small cell lung cancer (NSCLC) NCI-H1703 cell line that overexpressed PDGFRα, **15i** and imatinib only exhibited moderate inhibitory activity (GI_{50}: 5.37 μM and 2.1 μM, respectively). Upon stimulation of PDGFRα activity with PDGF AA (100 ng/mL), **15i** displayed slightly higher potency to NCI-H1703 cells (GI_{50}: 2.99 μM). The multiple targets imatinib also exhibited stronger inhibition under this condition (GI_{50}: 0.227 μM).

Next, we tested the effect of **15i** on PDGFRα mediated signaling pathways (Fig. 5). In EOL-1 cells, it strongly blocked PDGFRα Y1018 and Y849 auto-phosphorylation sites and downstream signaling mediators such as pSTAT3 (Y705), pSTAT5 (Y694) and pERK (T202/204). However, it showed no effect on pPDGFRα (Y754), which was the same with imatinib. In NCI-H1703 cells, PDGF AA stimulation was crucial for the PDGFRα mediated signaling. Without PDGF AA stimulation, auto-phosphorylation sites such as pPDGFRα (Y1018), pPDGFRα (Y754), pPDGFRα (Y849) and downstream signaling mediators such as pSTAT5 (Y694) and pAKT (T308) were barely detected (data not shown). However, with PDGF AA stimulation, **15i**'s dose-dependent inhibition of PDGFRα's auto-phosphorylation sites and downstream mediators were observed, *e. g.*, pPDGFRα (Y1018), pPDGFRα (Y754), pPDGFRα (Y849), pSTAT5 (Y694) and pERK (T202/Y204). Imatinib showed a similar trend.

In accordance to the results observed in the signaling pathway tests, **15i** could also effectively arrest the cell cycle into G0/G1 phase starting from a concentration of 0.01 μM in EOL-1 cells (Fig. 6A), indicating that **15i** mainly blocked cell proliferation through inhibition of cell growth. In NCI-H1703 cells, **15i** arrested the cell cycle into G0/G1 phase starting from 0.3 μM in a dose dependent manner and slightly stronger effects were observed upon PDGF AA (100 ng/mL) stimulation (Fig. 6B). In addition, **15i** could induce apoptosis in EOL-1 cells starting from a concentration of 3 nM by examining the cleavage of PARP and caspase-3 proteins (Fig. 7), indicating that the cells went to death through caspase-mediated programed cell death pathway. In NCI-H1703 cells, no apparent apoptosis was observed up to 10 μM of compound **15i.** However, upon stimulation of PDGFRα activity with PDGF AA (100 ng/mL), NCI-H1703 cells started to present dose-dependent apoptosis, which was in accordance to the growth inhibition assay and signaling investigation results of **15i**.

2.3. *In vivo* PK/PD evaluation

The pharmacokinetics properties of **15i** were evaluated in rats following intravenous and oral administration by using imatinib as control (Table 4). The results showed that **15i** exhibited comparable AUC value (527.5 versus 855.596 ng/ml*h) and half-life (2.05 versus 2.21 h) with imatinib. However, in oral administration, **15i** displayed poor oral bioavailability compared with imatinib (F: 1.96% versus 76.5%), which prevented it from oral gavage for *in vivo* study. Therefore, we tested **15i** in the EOL-1 xenograft mouse model for its anti-tumor efficacy with IP injection. As shown in Fig. 8 A, 25, 50 and 100 mpk dosages of **15i**

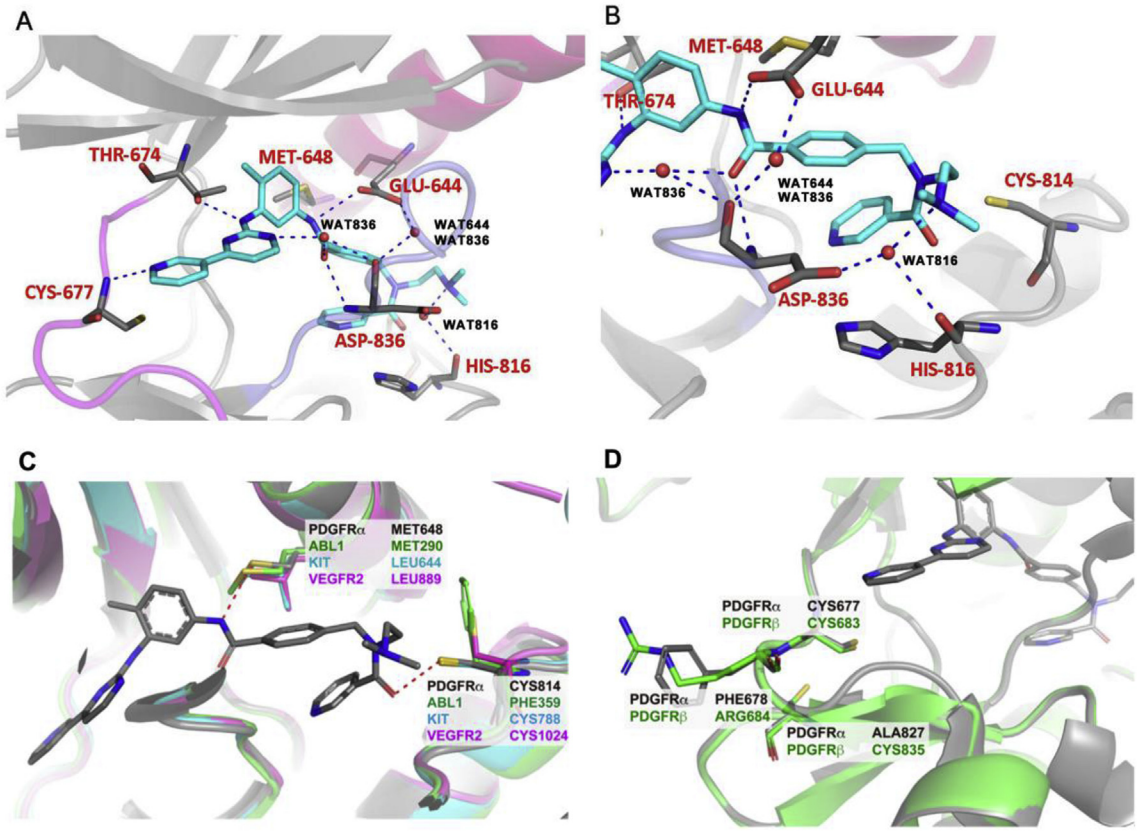

Fig. 4. Structure-based analysis of **15i**'s PDGFRα selectivity among structurally similar kinases. (A) X-ray crystal structure of **15i** in complex with PDGFRα (PDB ID: 5GRN). (B) Demonstration of distinct binding features of **15i** in complex with PDGFRα in the DFG-out shifting generated hydrophobic pocket. (C) Structure-based selectivity analysis of **15i** by docking to ABL1 kinase (PDB ID: 2E2B), c-KIT kinase (PDB ID: 4U0I) and VEGFR2 kinase (PDB ID: 3WZE). (D) Structure-based selectivity analysis of **15i** between PDGFRα/β by overlapping the X-ray structure of PDGFRα and the homology model of PDGFRβ built from it (PDB ID: 5GRN).

Table 3
Antiproliferative effect of compound **15i** on PDGFRα dependent/overexpressed cancer cell lines.[a]

Cell line	Imatinib (GI_{50}: μM)	Compd. **15i** (GI_{50}: μM)
EOL-1	<0.001	<0.001
NCI-H1703	2.10 ± 0.70	5.37 ± 0.14
NCI-H1703 + PDGF AA (100 ng/mL)	0.23 ± 0.03	2.99 ± 0.98

[a] All GI_{50} values (mean ± SD) were obtained by triplet testing and calculated using Prism 5.0 (GraphPad Software, San Diego, CA) by linear regression analysis.

and imatinib treatments both slightly affected the mice normal body weights. The difference of the weights between control mice and the drug treated mice was mainly due to significant tumor shrinkage. The TGI (tumor growth inhibition) with **15i** treatment at 25, 50 and 100 mpk were 71.5%, 95.4% and 100% respectively, which indicated **15i**'s considerable dose-dependent antitumor efficacy. At the same doses, imatinib exhibited stronger antitumor efficacy than **15i** in this animal model with the TGI of 99.9%, 100% and 100% respectively (Fig. 8B–D). Immunohistochemistry stain showed that **15i** could strongly suppress the tumor cell proliferation (Ki-67 stain) and induce the apoptosis (TUNEL stain) in the tumor tissues (Fig. 8 E).

In addition, to further examine the *in vivo* efficacy of **15i**, we tested it in the EOL-1 cell inoculated engraftment mouse model. As a result, **15i** exhibited similar efficacy to imatinib for the body weight control and survival rate at 30 mg/kg dosage (Fig. 9 A, B). It also displayed apparent dose-dependent survival rate improvement at the dosage of 7.5, 15 and 30 mg/kg/day respectively (Fig. 9 B), which was consistent with the flow cytometric results that **15i** could dose dependently reduce the EOL-1 cells in the bone marrow (Fig. 9C).

3. Conclusion

Starting from the known type II BCR-ABL/c-KIT/PDGFRs multi-target inhibitor imatinib, through medicinal chemistry exploration of the non-highly conserved DFG-out shifting generated allosteric hydrophobic pocket of the inactive conformation of PDGFRα kinase, we discovered a highly selective PDGFRα inhibitor compound **15i,** which displayed remarkable selectivity over structurally similar kinases such as PDGFRβ, ABL1, c-KIT and DDR1 etc. The newly obtained X-ray crystal structure of **15i** in complex with PDGFRα revealed a distinct binding feature that could partly explain its highly selective profile. Given the fact

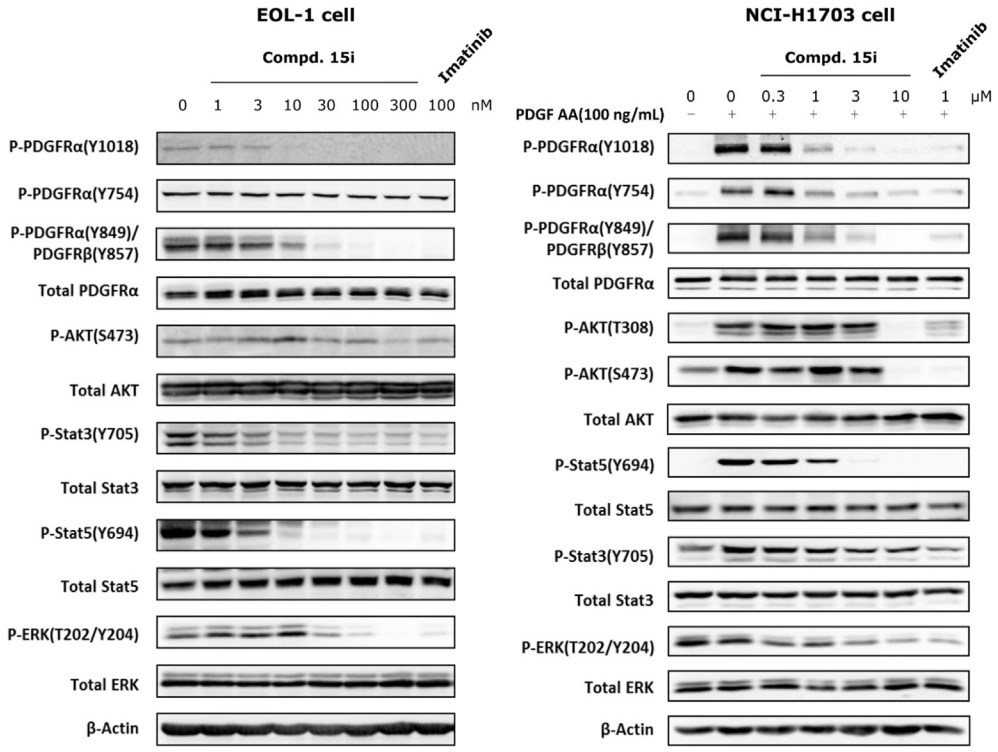

Fig. 5. Compound **15i**'s effects on the signaling transduction pathways in the PDGFRα dependent EOL-1 and PDGFRα overexpressed NCI-H1703 cell lines.

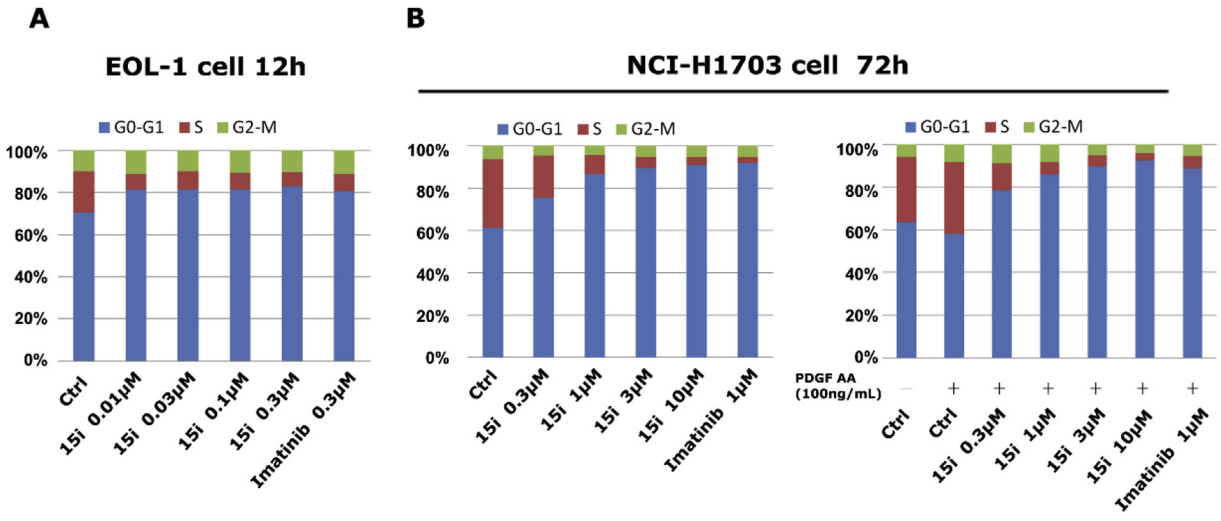

Fig. 6. Effect of compound **15**i on the cell cycle progression in (A) EOL-1 and (B) NCI-H1703 cell lines.

that currently the type II kinase inhibitors' pharmarcophore diversity was highly limited, this finding might provide a new approach to further expand the chemical scaffold diversity in the allosteric hydrophobic binding site to achieve better selectivity and activity. Compound **15i** strongly inhibited the cell proliferation, blocked the cell cycle progression and induced apoptosis in the PDGFRα dependent EOL-1 cancer cells. In addition, **15i** displayed great anti-tumor efficacy in EOL-1 cell inoculated xenograft mouse model and 100% TGI (tumor growth inhibition) was obtained with a dosage of 100 mg/kg/day. It also exhibited apparent survival improvement in the EOL-1 cell inoculated engraftment tumor model. The high selectivity and potency of compound **15i** suggested that it might be a useful pharmacological tool to further elucidate the pathology of PDGFRα in related cancers.

4. Experimental section

4.1. Chemistry

All reagents and solvents were purchased from commercial sources and used as obtained. ^{1}H NMR spectra were recorded with a Bruker 400 NMR spectrometer and referenced to deuterium dimethyl sulfoxide (DMSO-d6). Chemical shifts are expressed in ppm. In the NMR tabulation, s indicates singlet; d, doublet; t, triplet; q, quartet; m, multiplet and br, broad peak. High resolution

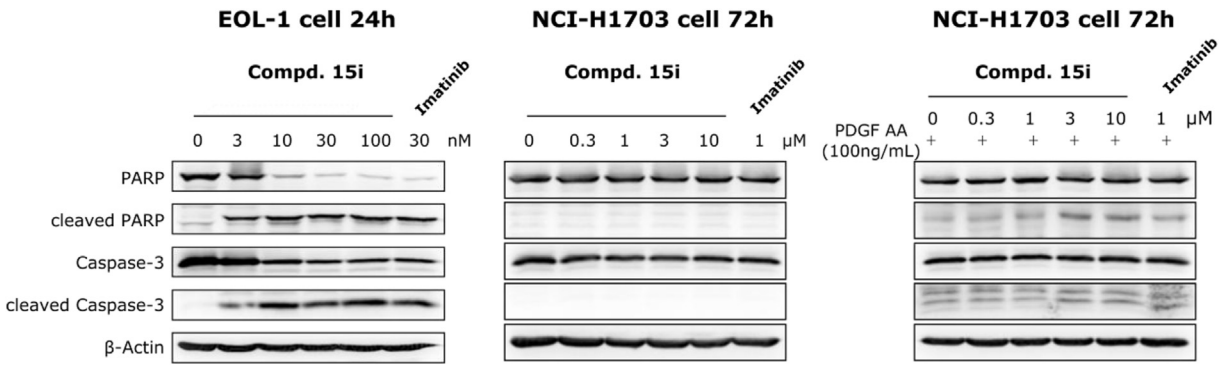

Fig. 7. Effect of compound **15i** on the apoptosis induction in EOL-1 and NCI-H1703 cell lines.

Table 4
Pharmacokinetic characterization of compounds **15i** and imatinib.

Compound	**15i**		Imatinib	
	IV (1 mg/kg)	PO (10 mg/kg)	IV (1 mg/kg)	PO (10 mg/kg)
AUC_{0-t} (ng/mL*h)	527.518 ± 161.345	103.411 ± 8.575	855.596 ± 17.968	6462.53 ± 2367.22
$AUC_{0-\infty}$ (ng/mL*h)	541.432 ± 156.628	115.46 ± 12.044	868.838 ± 203.044	6647.671 ± 2437.33
$MRT_{(0-t)}$ (h)	0.891 ± 0.297	3.328 ± 0.482	3.094 ± 1.098	7.454 ± 0.353
$T_{1/2}$ (h)	2.048 ± 0.483	2.031 ± 0.153	2.213 ± 0.564	4.262 ± 0.28
T_{max} (h)	0.017 ± 0	1.5 ± 0.707	0.017 ± 0	6.667 ± 1.155
Vz (L/kg)	5.982 ± 3.11	256.181 ± 45.957	3.696 ± 0.604	10.313 ± 4.55
CLz (L/h/kg)	1.962 ± 0.606	87.084 ± 9.083	1.191 ± 0.261	1.673 ± 0.701
C_{max} (ng/mL)	4591.968 ± 2333.519	28.91 ± 4.055	546.971 ± 20.351	531.349 ± 152.274
F (%)	N/A	1.96	N/A	76.51

mass spectrometry (HRMS) analysis was recorded on an Agilent 6224 Accurate-Mass TOF using an ESI source coupled to an Agilent 1260 Infinity HPLC system operating in reverse mode with an Agilent Eclipse Plus C18 1.8 μm 3.0 × 50 mm column. Flash column chromatography was conducted using silica gel (Silicycle 40–64 μm). The purities of all compounds were determined to be above 95% by HPLC.

*4.1.1. Compound **11b** was prepared following the synthetic procedure of **11a***

*4.1.1.1. 4-(Chloromethyl)-N-(4-methyl-3-((4-(pyridin-3-yl)pyrimidin-2-yl)amino)phenyl)benzamide (**11a**).*

6-Methyl-*N*-(4-(pyridin-3-yl)pyrimidin-2-yl)benzene-1,3-diamine (**10**) (5 mmol, 1.38 g) and DIEA (7.5 mmol, 968 mg) in 15 mL DMF at 0 °C was added 4-(chloromethyl)benzoyl chloride (5.5 mmol, 1.03 g) dropwisely, and the solution was stirred at 0 °C for 1 h. The system was quenched with water and extracted with EtOAc and dried with anhydrous Na_2SO_4. The solvents were removed under vacuum and the residue was purified by silica gel flash chromatography (EtOAc) to provide compound **11a** (1.84 g, 86%). ^{1}H NMR (400 MHz, DMSO-d6) δ 10.29 (s, 1H), 9.29 (s, 1H), 8.98 (s, 1H), 8.69 (s, 1H), 8.52 (s, 2H), 8.12 (s, 1H), 7.99 (s, 2H), 7.70–7.33 (m, 5H), 7.22 (s, 1H), 4.85 (s, 2H), 2.24 (s, 3H). ^{13}C NMR (101 MHz, DMSO-d6): δ 164.95, 161.53, 161.08, 159.36, 151.21, 148.05, 140.83, 137.73, 137.05, 134.78, 134.43, 132.15, 130.00, 128.64,128.02, 127.64, 123.73, 117.23, 116.87, 107.51, 45.41, 17.60. HRMS (ESI, *m/z*) $[M+H]^+$ calcd for $C_{24}H_{21}ClN_5O$: 430.1435, found: 430.1436 [21].

*4.1.1.2. 3-(Chloromethyl)-N-(4-methyl-3-((4-(pyridin-3-yl)pyrimidin-2-yl)amino)phenyl)benzamide (**11b**).* Yield 83%. ^{1}H NMR (400 MHz, DMSO-d6) δ 10.29 (s, 1H), 9.28 (s, 1H), 9.00 (s, 1H), 8.68 (d, *J* = 4.6 Hz, 1H), 8.52–8.47 (m, 2H), 8.08 (s, 1H), 8.01 (s, 1H), 7.93 (d, *J* = 7.6 Hz, 1H), 7.65 (d, *J* = 6.7 Hz, 1H), 7.62–7.47 (m, 3H), 7.43 (d, *J* = 5.1 Hz, 1H), 7.21 (d, *J* = 8.1 Hz, 1H), 4.86 (s, 2H), 2.22 (s, 3H). ^{13}C NMR (101 MHz, DMSO-d6) δ 170.32, 166.55, 164.84, 156.48, 153.35, 143.28, 143.15, 142.50, 140.79, 140.05, 137.63, 137.15, 135.40, 134.10, 133.59, 132.96, 129.24, 122.72, 122.29, 112.92, 51.13, 23.05. HRMS (ESI, *m/z*) $[M+H]^+$ calcd for $C_{24}H_{21}ClN_5O$: 430.1435, found: 430.1438.

*4.1.2. tert-Butyl 4-((4-methyl-3-((4-(pyridin-3-yl)pyrimidin-2-yl)amino)phenyl)carbamoyl)-2-(trifluoromethyl)benzylcarbamate (**11c**)*

6-Methyl-N-(4-(pyridin-3-yl)pyrimidin-2-yl)benzene-1,3-diamine (**10**) (5 mmol, 1.38 g) and 4-(((tert-butoxycarbonyl)amino)methyl)-3-(trifluoromethyl)benzoic acid (5 mmol, 1.6 g) in 15 mL DMF and HATU (6 mmol, 2.28 g), DIEA (10 mmol, 1.29 g) were stirred at room temperature overnight, and then the system was quenched with water, extracted with EtOAc and dried with anhydrous Na_2SO_4. The solvents were removed under vacuum and the residue was purified by silica gel flash chromatography (DCM: MeOH = 15: 1) to give product **11c** (2.37 g, yield 82%). ^{1}H NMR (400 MHz, DMSO-d6) δ 10.41 (s, 1H), 9.29 (s, 1H), 8.99 (s, 1H), 8.69 (s, 1H), 8.51 (s, 2H), 8.26 (s, 2H), 8.09 (s, 1H), 7.78–7.37 (m, 5H), 7.24 (s, 1H), 4.40 (s, 2H), 2.25 (s, 3H), 1.43 (s, 9H). HRMS (ESI, *m/z*) $[M+H]^+$ calcd for $C_{30}H_{30}F_3N_6O_3$: 579.2331, found: 579.2336.

*4.1.3. Compound **12b** was prepared following the synthetic procedure of **12a***

*4.1.3.1. 4-(Aminomethyl)-N-(4-methyl-3-((4-(pyridin-3-yl)pyrimidin-2-yl)amino)phenyl)benzamide (**12a**).* Compound **11a** (4 mmol, 1.71 g) and NaN_3 (6 mmol, 0.39 g) in DMF 10 mL were stirred at room temperature overnight and the system was extracted with EtOAc, then the solvent was concentrated to 20 mL and Pd/C (5%) was added. The mixture was stirred under H_2 at room temperature for 6 h. The system was filtered by diatomaceous earth and the filtrate was concentrated under vacuum. The residue was purified by silica gel flash chromatography (DCM: MeOH = 15: 1) to

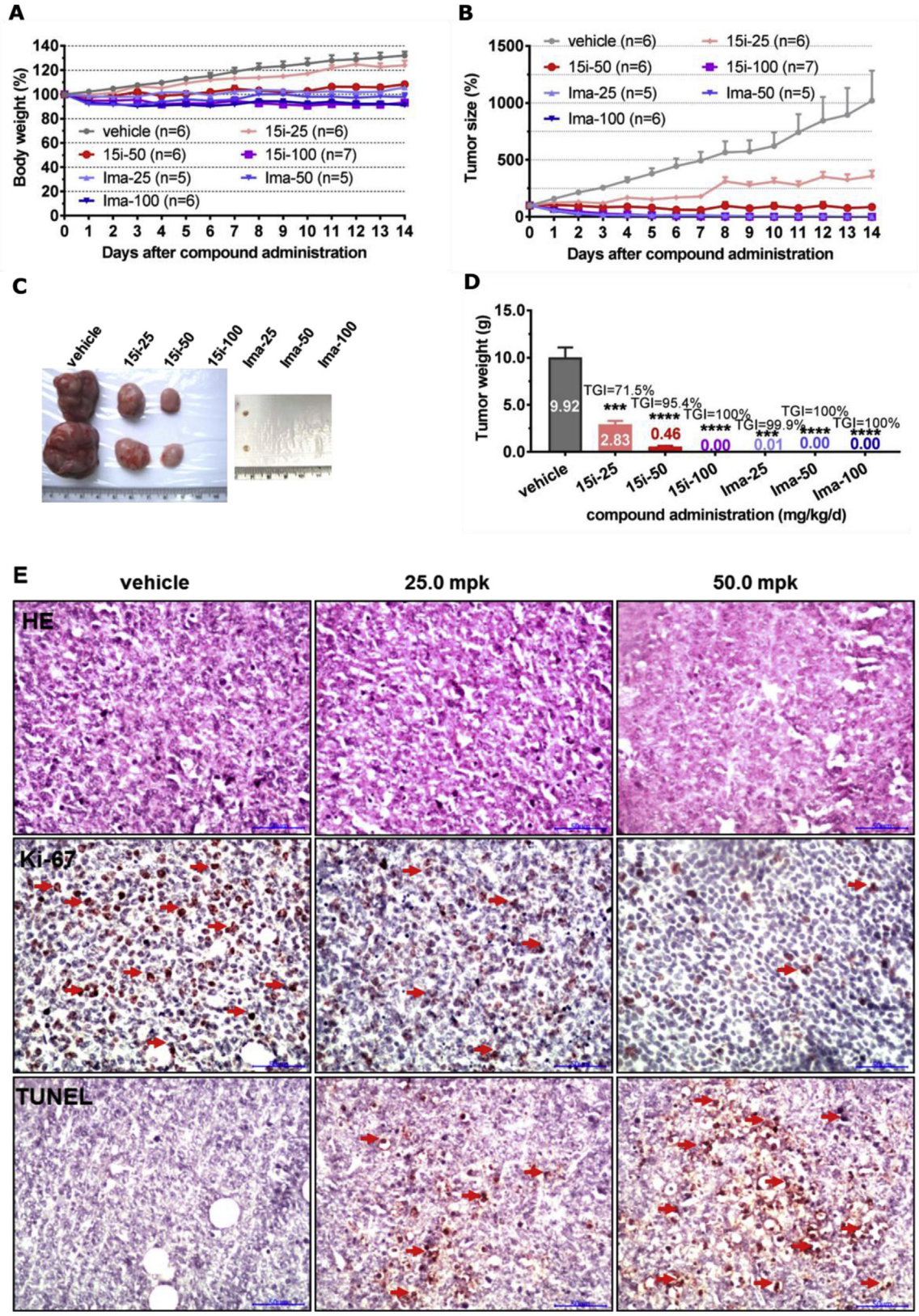

Fig. 8. Compound **15i** and imatinib's anti-tumor efficacy in EOL-1 xenograft mouse model. Female nu/nu mice bearing established EOL-1 tumor xenografts were treated with **15i** and imatinib at 25.0, 50.0 and 100 mg/kg/d, or vehicle. Daily IP injection was initiated when EOL-1 tumors had reached a size of 200–400 mm^3. Each group contained 6 animals. Data, mean ± SEM. (A) Body weight. (B) Tumor size measurements from EOL-1 xenograft mice after **15i** and imatinib administration. Initial body weight and tumor size were set as 100%. (C) Representative photographs of tumors in each group after 25.0, 50.0 or 100 mg/kg/d **15i** and imatinib or vehicle treatment. (D) Comparison of the final tumor weight in each group after 14-day treatment period of **15i** and imatinib. Numbers in columns indicate the mean tumor weight in each group. ns, $p > 0.05$, $^{*}p < 0.05$, $^{**}p < 0.01$. (E) Representative micrographs of hematoxylin and eosin (HE), Ki-67, and TUNEL staining of tumor tissues with **15i** treatment groups in comparison with the vehicle treatment group. Note the specific nuclear staining of cells with morphology consistent with proliferation and apoptosis (E, red arrow). (For interpretation of the references to colour in this figure legend, the reader is referred to the Web version of this article.)

give compound **12a** (1.13 g, two-step yield 69%). ^{1}H NMR (400 MHz, DMSO-d6) δ 10.15 (s, 1H), 9.28 (s, 1H), 8.99 (s, 1H), 8.69 (s, 1H), 8.51 (d, J = 4.0 Hz, 2H), 8.09 (s, 1H), 7.92 (d, J = 6.2 Hz, 2H), 7.61–7.33 (m, 5H), 7.20 (d, J = 7.8 Hz, 1H), 4.13 (s, 2H),2.23 (s, 3H). HRMS (ESI, m/z) $[M+H]^+$ calcd for $C_{24}H_{23}N_6O$: 411.1933, found: 411.1936 [20].

*4.1.3.2. 3-(Aminomethyl)-N-(4-methyl-3-((4-(pyridin-3-yl)pyrimidin-2-yl)amino)phenyl)benzamide (**12b**).* Two-step yield 62%. ^{1}H NMR (400 MHz, DMSO-d6) δ 10.19 (s, 1H), 9.28 (s, 1H), 8.98 (s, 1H), 8.69 (s, 1H), 8.51 (s, 2H), 8.15–7.74 (m, 3H), 7.61–7.39 (m, 5H), 7.22 (s, 1H), 3.81 (s, 2H), 2.23 (s, 3H). ^{13}C NMR (101 MHz, DMSO-d6) δ 170.99, 166.98, 166.58, 164.83, 156.72, 153.56, 149.41, 143.17, 142.66, 140.32, 139.80, 137.60, 135.39, 133.46, 132.98, 131.82, 131.03, 129.15, 122.68, 122.22, 112.89, 50.74, 23.04. HRMS (ESI, m/z) $[M+H]^+$ calcd for $C_{24}H_{23}N_6O$: 411.1933, found: 411.1936.

*4.1.4. 4-(Aminomethyl)-N-(4-methyl-3-((4-(pyridin-3-yl)pyrimidin-2-yl)amino)phenyl)-3-(trifluoromethyl)benzamide **(12c)***

Compound **11c** (1 mmol, 578 mg) was dissolved in 4 N HCl in EtOAc (5 mL). The system was stirred at room temperature for 6 h, and then neutralized by aqueous $NaHCO_3$. The organic phase was collected and the solvent was removed by rotary evaporator to afford compound **12c**, which was used in the next step directly. Two-step yield 56%. ^{1}H NMR (400 MHz, DMSO-d6) δ 10.39 (s, 1H), 9.29 (s, 1H), 8.99 (s, 1H), 8.69 (s, 1H), 8.51 (d, J = 12.1 Hz, 2H), 8.24 (s, 2H), 8.10 (s, 1H), 7.99 (s, 1H), 7.51–7.44 (m, 3H), 7.24 (s, 1H), 3.97 (s, 2H), 2.25 (s, 3H). HRMS (ESI, m/z) $[M+H]^+$ calcd for $C_{25}H_{22}F_3N_6O$: 479.1807, found: 479.1802.

*4.1.5. Compounds **12e-f** were prepared following the synthetic procedure of **12d***

*4.1.5.1. 4-Amino-N-(4-methyl-3-((4-(pyridin-3-yl)pyrimidin-2-yl)amino)phenyl)benzamide (**12d**).*

6-methyl-*N*-(4-(pyridin-3-yl)pyrimidin-2-yl)benzene-1,3-diamine (**10**) (5 mmol, 1.38 g) and 4-nitro-benzoic acid (5 mmol, 0.84 g) in 15 mL DMF and HATU (6 mmol, 2.28 g), DIEA (10 mmol, 1.29 g) were stirred at room temperature overnight. Then the system was quenched with water, extracted with EtOAc and dried with anhydrous Na_2SO_4. The solvents were removed under vacuum to give compound **11d**. HRMS (ESI, m/z) $[M+H]^+$ calcd for $C_{23}H_{19}N_6O_3$: 427.1519, found: 427.1518. The crude product **11d** (4 mmol, 1.70 g) was directly dissolved in 20 mL EtOAc and Pd/C (5%) was added. The mixture was stirred under H_2 at room temperature for 6 h, then the system was filtered by diatomaceous earth and the filtrate was concentrated under vacuum. The residue was purified by silica gel flash chromatography (DCM: MeOH = 15: 1) to yield product **12d** (1.52 g, two-step yield 79%). ^{1}H NMR (400 MHz, DMSO-d6) δ 9.72 (s, 1H), 9.27 (s, 1H), 8.96 (s, 1H), 8.68 (d, J = 4.7 Hz, 1H), 8.55–8.36 (m, 2H), 8.03 (s, 1H), 7.73 (t, J = 15.2 Hz, 2H), 7.53–7.41 (m, 3H), 7.16 (d, J = 8.2 Hz, 1H), 6.59 (d, J = 8.5 Hz, 2H), 5.74 (s, 2H), 2.20 (s, 3H). ^{13}C NMR (101 MHz, DMSO-d6) δ 170.99, 166.98, 166.58, 164.83, 156.72, 153.56, 149.41, 143.17, 142.66, 140.32, 139.80, 137.60, 135.39, 133.46, 132.98, 131.82, 131.03, 129.15, 122.68, 122.22, 112.89, 50.74, 23.04. HRMS (ESI, m/z) $[M+H]^+$ calcd for $C_{23}H_{21}N_6O$: 397.1777, found: 397.1773.

*4.1.5.2. 3-Amino-N-(4-methyl-3-((4-(pyridin-3-yl)pyrimidin-2-yl)amino)phenyl)benzamide (**12e**).* Two-step yield 76%. ^{1}H NMR (400 MHz, DMSO-d6) δ 10.04 (s, 1H), 9.28 (s, 1H), 8.97 (s, 1H), 8.69 (s, 1H), 8.51 (s, 2H), 8.08 (s, 1H), 7.57–7.36 (m, 3H), 7.20–7.10 (m, 4H), 6.75 (s, 1H), 5.31 (s, 2H), 2.22 (s, 3H). ^{13}C NMR (101 MHz, DMSO-d6) δ 168.52, 167.04, 166.53, 164.84, 156.75, 153.58, 153.11, 143.33, 142.10, 141.82, 139.81, 139.53, 137.59, 135.53, 133.39, 131.39, 129.14, 127.81, 122.68, 122.30, 113.00, 23.06. HRMS (ESI, m/z) $[M+H]^+$ calcd for $C_{23}H_{21}N_6O$: 397.1777, found: 397.1772.

*4.1.5.3. 3-Amino-N-(4-methyl-3-((4-(pyridin-3-yl)pyrimidin-2-yl)amino)phenyl)-5-(trifluoromethyl)benzamide (**12f**).* Two-step yield 72%. ^{1}H NMR (400 MHz, DMSO-d6) δ 10.25 (s, 1H), 9.29 (s, 1H), 8.99 (s, 1H), 8.70 (s, 1H), 8.52 (s, 2H), 8.08 (s, 1H), 7.52–7.37 (m, 5H), 7.22 (s, 1H), 7.04 (s, 1H), 5.86 (s, 2H), 2.24 (s, 3H). ^{13}C NMR (101 MHz, DMSO-d6) δ 168.52, 167.04, 166.53, 164.84, 156.75, 153.58, 153.11, 143.33, 142.10, 141.82, 139.81, 139.53, 137.59, 135.53, 133.39, 131.39, 129.14, 127.81, 122.68, 122.30, 113.00, 23.06. HRMS (ESI, m/z) $[M+H]^+$ calcd for $C_{24}H_{20}F_3N_6O$: 465.1651, found: 465.1657.

*4.1.6. Compounds **13b-n** were prepared following the synthetic procedure of **13a***

*4.1.6.1. N-(4-methyl-3-((4-(pyridin-3-yl)pyrimidin-2-yl)amino)phenyl)-4-(propionamidomethyl)benzamide (**13a**).* Compound **12a** (0.05 mmol, 20 mg) and DIEA (0.075 mmol, 9.75 mg) were dissolved in 0.5 mL of DMF and cooled to 0 °C, then propionyl chloride (0.06 mmol, 5.5 mg) was added to the system and the mixture was stirred at 0 °C for 1 h. The system was extracted with EtOAc and dried with anhydrous Na_2SO_4. The solvents were removed under vacuum and the residue was purified by silica gel flash chromatography (DCM: MeOH = 15: 1) to afford compound **13a** (15 mg, yield 65%). ^{1}H NMR (400 MHz, DMSO-d6) δ 10.17 (d, J = 20.7 Hz, 1H), 9.27 (s, 1H), 8.96 (s, 1H), 8.68 (d, J = 4.6 Hz, 1H), 8.49 (dd, J = 13.9, 6.6 Hz, 2H), 8.35 (t, J = 5.9 Hz, 1H), 8.19–7.95 (m, 1H), 7.93 (t, J = 11.1 Hz, 2H), 7.60–7.30 (m, 5H), 7.21 (d, J = 8.3 Hz, 1H), 4.33 (d, J = 5.9 Hz, 2H), 2.23 (s, 3H), 2.17 (q, J = 7.6 Hz, 2H), 1.11–0.94 (m, 3H). HRMS (ESI, m/z) $[M+H]^+$ calcd for $C_{27}H_{27}N_6O_2$: 467.2195, found: 467.2189.

*4.1.6.2. 4-(Acrylamidomethyl)-N-(4-methyl-3-((4-(pyridin-3-yl)pyrimidin-2-yl)amino)phenyl)benzamide (**13b**).* Yield 63%. ^{1}H NMR (400 MHz, DMSO-d6) δ 10.18 (s, 1H), 9.28 (s, 1H), 8.98 (s, 1H), 8.83–8.58 (m, 2H), 8.49 (dd, J = 13.2, 6.5 Hz, 2H), 8.08 (s, 1H), 7.92 (d, J = 8.1 Hz, 2H), 7.59–7.29 (m, 5H), 7.20 (d, J = 8.3 Hz, 1H), 6.31 (dd, J = 17.1, 10.2 Hz, 1H), 6.14 (dd, J = 17.1, 1.9 Hz, 1H), 5.64 (dd, J = 10.1, 1.8 Hz, 1H), 4.43 (d, J = 6.0 Hz, 2H), 2.22 (s, 3H). HRMS (ESI, m/z) $[M+H]^+$ calcd for $C_{27}H_{25}N_6O_2$: 465.2039, found: 465.2033.

*4.1.6.3. N-(4-Methyl-3-((4-(pyridin-3-yl)pyrimidin-2-yl)amino)phenyl)-4-(vinylsulfonamidomethyl)benzamide (**13c**).* Yield 75%. ^{1}H NMR (400 MHz, DMSO-d6) δ 10.25 (s, 1H), 9.27 (s, 1H), 8.97 (s, 1H), 8.68 (d, J = 4.3 Hz, 1H), 8.49 (dd, J = 11.6, 6.5 Hz, 2H), 8.01 (dd, J = 40.0, 20.5 Hz, 4H), 7.61–7.33 (m, 5H), 7.20 (d, J = 8.3 Hz, 1H), 6.71 (dd, J = 16.5, 10.0 Hz, 1H), 6.00 (dd, J = 35.1, 13.2 Hz, 2H), 4.14 (s, 2H), 2.22 (s, 3H). HRMS (ESI, m/z) $[M+H]^+$ calcd for $C_{26}H_{25}N_6O_3S$: 501.1709, found: 501.1706.

*4.1.6.4. N-(4-((4-Methyl-3-((4-(pyridin-3-yl)pyrimidin-2-yl)amino)phenyl)carbamoyl)benzyl)nicotinamide (**13d**).* ^{1}H NMR (400 MHz, DMSO-d6) δ 10.18 (s, 1H), 9.28 (s, 2H), 9.08 (s, 1H), 8.98 (s, 1H), 8.70 (s, 2H), 8.52 (s, 2H), 8.26 (s, 1H), 8.09 (s, 1H), 7.95 (s, 2H), 7.50 (s, 6H), 7.22 (s, 1H), 4.60 (s, 2H), 2.23 (s, 3H). HRMS (ESI, m/z) $[M+H]^+$ calcd for $C_{30}H_{26}N_7O_2$: 516.2148, found: 516.2152.

*4.1.6.5. N-(4-Methyl-3-((4-(pyridin-3-yl)pyrimidin-2-yl)amino)phenyl)-3-(propionamidomethyl)benzamide (**13e**).* Yield 71%. ^{1}H NMR (400 MHz, DMSO-d6) δ 10.22 (s, 1H), 9.28 (s, 1H), 8.99 (s, 1H), 8.68 (s, 1H), 8.56–8.39 (m, 2H), 8.36 (s, 1H), 8.08 (s, 1H), 7.82 (s, 2H), 7.59–7.34 (m, 5H), 7.21 (d, J = 7.7 Hz, 1H), 4.34 (s, 2H), 2.26–2.03 (m, 5H), 1.03–0.97 (m, 3H). HRMS (ESI, m/z) $[M+H]^+$ calcd for $C_{27}H_{27}N_6O_2$: 467.2195, found: 467.2189.

*4.1.6.6. 3-(Acrylamidomethyl)-N-(4-methyl-3-((4-(pyridin-3-yl)pyrimidin-2-yl)amino)phenyl)benzamide (**13f**).* Yield 69%. ^{1}H NMR (400 MHz, DMSO-d6) δ 10.24 (s, 1H), 9.27 (s, 1H), 8.98 (s, 1H), 8.69

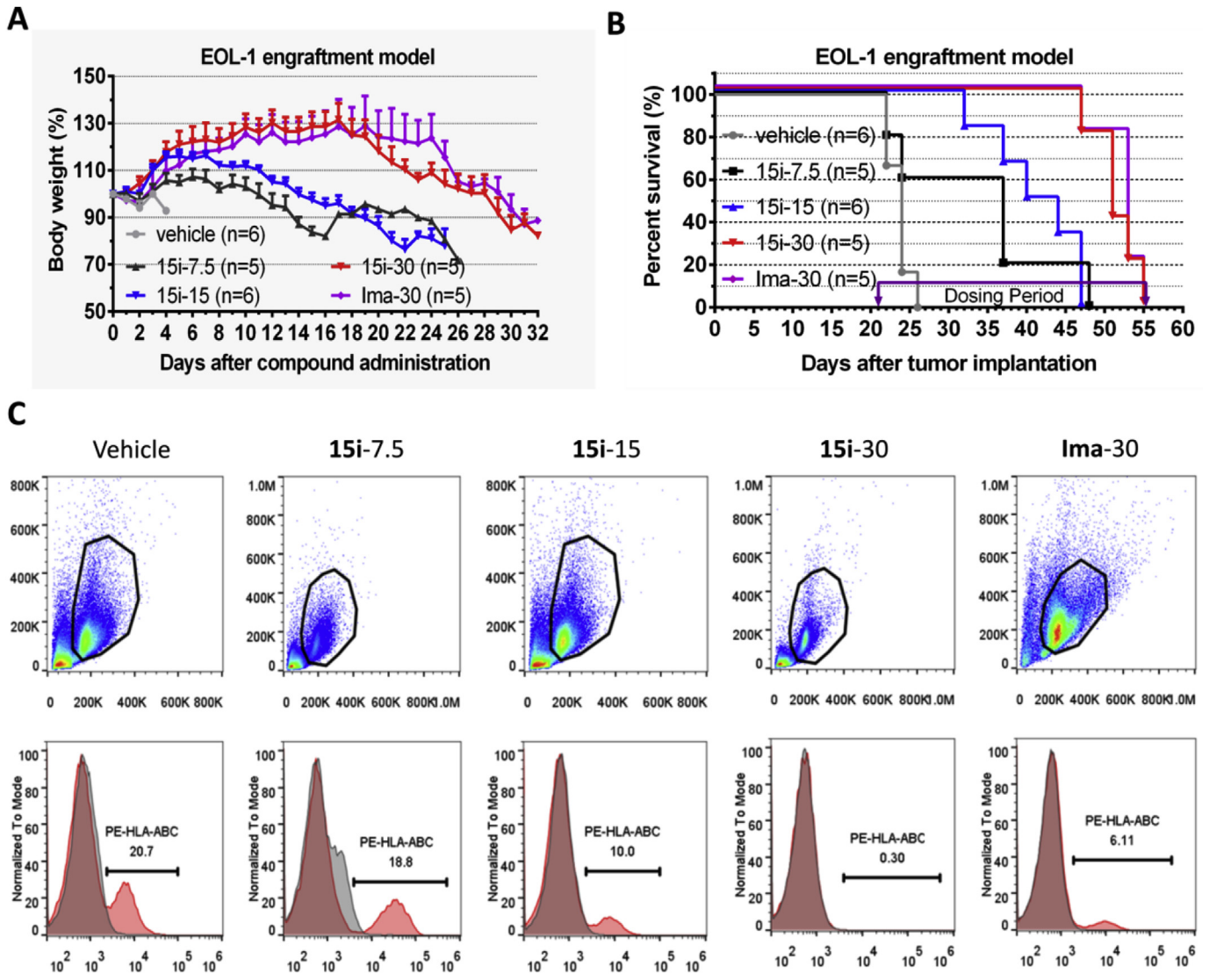

Fig. 9. Compound **15i** and imatinib's efficacy in EOL-1 cell inoculated engraftment mouse model (dosage: mg/kg/day). (A) Body weights after **15i**/imatinib administration. (B) Survival experiment of EOL-1 engraftment mice after **15i**/imatinib administration. (C) FACS detection of EOL-1 cells in the bone marrow in the mouse models.

(s, 2H), 8.50 (d, $J = 4.8$ Hz, 2H), 8.08 (s, 1H), 7.85 (s, 2H), 7.45 (d, $J = 19.0$ Hz, 5H), 7.21 (s, 1H), 6.30 (s, 1H), 6.15 (d, $J = 4.8$ Hz, 1H), 5.62 (s, 1H), 4.43 (s, 2H), 2.22 (s, 3H). HRMS (ESI, *m/z*) $[M+H]^+$ calcd for $C_{27}H_{25}N_6O_2$: 465.2039, found: 465.2034.

*4.1.6.7. 4-(Acrylamidomethyl)-N-(4-methyl-3-((4-(pyridin-3-yl)pyrimidin-2-yl)amino)phenyl)-3-(trifluoromethyl)benzamide (**13g**).* Yield 66%. ^{1}H NMR (400 MHz, DMSO-d6) δ 10.41 (s, 1H), 9.28 (d, $J = 1.7$ Hz, 1H), 8.98 (s, 1H), 8.80 (t, $J = 5.8$ Hz, 1H), 8.68 (dd, $J = 4.7$, 1.5 Hz, 1H), 8.56–8.42 (m, 2H), 8.35–8.14 (m, 2H), 8.08 (s, 1H), 7.63 (d, $J = 8.1$ Hz, 1H), 7.48 (ddd, $J = 19.5$, 12.8, 5.0 Hz, 3H), 7.23 (d, $J = 8.3$ Hz, 1H), 6.36 (dd, $J = 17.1$, 10.2 Hz, 1H), 6.17 (dd, $J = 17.1$, 2.0 Hz, 1H), 5.68 (dd, $J = 10.2$, 2.0 Hz, 1H), 4.59 (d, $J = 5.5$ Hz, 2H), 2.23 (s, 3H). HRMS (ESI, *m/z*) $[M+H]^+$ calcd for $C_{28}H_{24}F_3N_6O_2$: 533.1913, found: 533.1916.

*4.1.6.8. N-(4-((4-Methyl-3-((4-(pyridin-3-yl)pyrimidin-2-yl)amino)phenyl)carbamoyl)-2-(trifluoromethyl)benzyl)nicotinamide (**13h**).* Yield 73%. ^{1}H NMR (400 MHz, DMSO-d6) δ 10.42 (s, 1H), 9.42 (s, 1H), 9.28 (s, 1H), 9.12 (s, 1H), 8.99 (s, 1H), 8.77–8.49 (m, 4H), 8.33–8.22 (m, 3H), 8.09 (s, 1H), 7.74 (s, 1H), 7.62–7.39 (m, 4H), 7.24 (s, 1H), 4.76 (s, 2H), 2.24 (s, 3H). HRMS (ESI, *m/z*) $[M+H]^+$ calcd for $C_{31}H_{25}F_3N_7O_2$:584.2022, found: 584.2018.

*4.1.6.9. N-(4-Methyl-3-((4-(pyridin-3-yl)pyrimidin-2-yl)amino)phenyl)-4-propionamidobenzamide (**13i**).* Yield 65%. ^{1}H NMR (400 MHz, DMSO-d6) δ 10.16 (s, 1H), 10.07 (s, 1H), 9.29 (s, 1H), 8.97 (s, 1H), 8.70 (s, 1H), 8.51 (dd, $J = 9.0$, 5.5 Hz, 2H), 8.08 (s, 1H), 8.01–7.84 (m, 2H), 7.73 (d, $J = 7.0$ Hz, 2H), 7.48 (dd, $J = 21.4$, 15.7 Hz, 3H), 7.21 (d, $J = 9.8$ Hz, 1H), 2.38 (s, 2H), 2.23 (s, 3H), 1.10 (s, 3H). HRMS (ESI, *m/z*) $[M+H]^+$ calcd for $C_{26}H_{25}N_6O_2$: 453.2039, found: 453.2036.

*4.1.6.10. 4-Acrylamido-N-(4-methyl-3-((4-(pyridin-3-yl)pyrimidin-2-yl)amino)phenyl)benzamide (**13j**).* Yield 56%. ^{1}H NMR (400 MHz, DMSO-d6) δ 10.52 (s, 1H), 10.11 (s, 1H), 9.28 (s, 1H), 8.98 (s, 1H), 8.68 (s, 1H), 8.59–8.39 (m, 2H), 8.08 (s, 1H), 7.95 (s, 2H), 7.82 (d, $J = 6.7$ Hz, 2H), 7.56–7.35 (m, 3H), 7.20 (d, $J = 7.0$ Hz, 1H), 6.60–6.35 (m, 1H), 6.30 (d, $J = 16.8$ Hz, 1H), 5.81 (d, $J = 9.4$ Hz, 1H), 2.22 (s, 3H). HRMS (ESI, *m/z*) $[M+H]^+$ calcd for $C_{26}H_{23}N_6O_2$: 451.1882, found: 451.1883.

*4.1.6.11. N-(4-((4-Methyl-3-((4-(pyridin-3-yl)pyrimidin-2-yl)amino) phenyl)carbamoyl)phenyl)nicotinamide (**13k**).* Yield 72%. ^{1}H NMR (400 MHz, DMSO-d6) δ 10.71 (s, 1H), 10.15 (s, 1H), 9.29 (s, 1H), 9.15 (s, 1H), 8.98 (s, 1H), 8.70 (s, 2H), 8.52 (s, 2H), 8.35 (s, 1H), 8.10–7.95 (m, 5H), 7.60–7.45 (m, 4H), 7.23 (s, 1H), 2.24 (s, 3H). HRMS (ESI, *m*/*z*) $[M+H]^+$ calcd for $C_{29}H_{24}N_7O_2$: 502.1991, found: 502.1987.

*4.1.6.12. 3-Acrylamido-N-(4-methyl-3-((4-(pyridin-3-yl)pyrimidin-2-yl)amino)phenyl)benzamide (**13l**).* Yield 55%. ^{1}H NMR (400 MHz, DMSO-d6) δ 10.38 (s, 1H), 10.23 (s, 1H), 9.27 (s, 1H), 8.98 (s, 1H), 8.68 (s, 1H), 8.50 (dd, *J* = 10.5, 5.9 Hz, 2H), 8.16 (s, 1H), 8.07 (s, 1H), 7.92 (s, 1H), 7.65 (s, 1H), 7.48 (t, *J* = 22.1 Hz, 4H), 7.21 (d, *J* = 7.7 Hz, 1H), 6.64–6.33 (m, 1H), 6.29 (d, *J* = 16.7 Hz, 1H), 5.79 (d, *J* = 7.8 Hz, 1H), 2.23 (s, 3H). HRMS (ESI, *m*/*z*) $[M+H]^+$ calcd for $C_{26}H_{23}N_6O_2$: 451.1882, found: 451.1886.

*4.1.6.13. 3-Acrylamido-N-(4-methyl-3-((4-(pyridin-3-yl)pyrimidin-2-yl)amino)phenyl)-5-(trifluoromethyl)benzamide (**13m**).* Yield 67%. ^{1}H NMR (400 MHz, DMSO-d6) δ 10.94 (s, 1H), 10.49 (s, 1H), 9.31 (s, 1H), 9.00 (s, 1H), 8.72 (s, 1H), 8.51 (dd, *J* = 13.1, 6.6 Hz, 2H), 8.43 (d, *J* = 5.5 Hz, 2H), 8.08 (s, 1H), 8.03 (s, 1H), 7.61–7.37 (m, 3H), 7.25 (d, *J* = 8.3 Hz, 1H), 6.54 (dd, *J* = 17.1, 10.1 Hz, 1H), 6.35 (d, *J* = 16.7 Hz, 1H), 5.85 (d, *J* = 10.1 Hz, 1H), 2.25 (s, 3H). HRMS (ESI, *m*/*z*) $[M+H]^+$ calcd for $C_{27}H_{22}F_3N_6O_2$: 519.1756, found: 519.1751.

*4.1.6.14. N-(4-Methyl-3-((4-(pyridin-3-yl)pyrimidin-2-yl)amino) phenyl)-3-propionamido-5-(trifluoromethyl)benzamide (**13n**).* Yield 72%. ^{1}H NMR (400 MHz, DMSO-d6) δ 10.44 (s, 2H), 9.28 (d, *J* = 1.5 Hz, 1H), 9.01 (s, 1H), 8.75–8.61 (m, 1H), 8.51 (dd, *J* = 15.3, 6.6 Hz, 2H), 8.34 (s, 1H), 8.30 (s, 1H), 8.07 (s, 1H), 7.99 (s, 1H), 7.50 (ddd, *J* = 20.3, 9.9, 5.0 Hz, 3H), 7.24 (d, *J* = 8.4 Hz, 1H), 4.04 (dd, *J* = 13.5, 6.5 Hz, 1H), 2.40 (q, *J* = 7.5 Hz, 2H), 2.25 (s, 3H), 1.12 (t, *J* = 7.5 Hz, 3H). HRMS (ESI, *m*/*z*) $[M+H]^+$ calcd for $C_{27}H_{24}F_3N_6O_2$: 521.1913, found: 521.1917.

*4.1.7. Compounds **14b-e** were prepared following the synthetic procedure of **14a***

*4.1.7.1. 4-(((2-(Dimethylamino)ethyl)amino)methyl)-N-(4-methyl-3-((4-(pyridin-3-yl)pyrimidin-2-yl)amino)phenyl)benzamide (**14a**).* Compound **11a** (5 mmol, 2.14 g) and N^1,N^1-dimethylethane-1,2-diamine (15 mmol, 1.32 g) in 15 mL DMF were stirred at room temperature overnight. The solvents were removed under vacuum and the residue was purified by silica gel flash chromatography (DCM: MeOH = 10: 1) to give compound **14a** (1.9 g, yield 79%). ^{1}H NMR (400 MHz, DMSO-d6) δ 10.19 (s, 1H), 9.27 (s, 1H), 8.97 (s, 1H), 8.68 (s, 1H), 8.51–8.47 (m, 2H), 8.09 (s, 1H), 7.95 (s, 2H), 7.63–7.32 (m, 5H), 7.20 (s, 1H), 3.91 (s, 2H), 2.74 (s, 2H), 2.63 (s, 2H), 2.33 (s, 6H), 2.22 (s, 3H). ^{13}C NMR (101 MHz, DMSO-d6) δ 165.57, 162.07, 161.67, 159.94, 151.84, 148.66, 142.36, 138.25, 137.67, 134.90, 134.33, 132.69, 130.46, 128.86, 128.13, 124.25, 117.80, 117.32, 107.98, 57.17, 51.99, 45.07, 44.88, 18.13. HRMS (ESI, *m*/*z*) $[M+H]^+$ calcd for $C_{28}H_{32}N_7O$: 482.2668, found: 482.2663.

*4.1.7.2. 4-((Isopentylamino)methyl)-N-(4-methyl-3-((4-(pyridin-3-yl)pyrimidin-2-yl)amino)phenyl)benzamide (**14b**).* Yield 86%. ^{1}H NMR (400 MHz, DMSO-d6) δ 10.23 (s, 1H), 9.29 (s, 1H), 8.98 (s, 1H), 8.69 (s, 1H), 8.52 (s, 2H), 8.22–7.83 (m, 4H), 7.61–7.44 (m, 5H), 7.22 (d, *J* = 6.3 Hz, 1H), 4.01 (s, 2H), 2.74 (s, 2H), 2.24 (s, 3H), 1.63 (s, 1H), 1.47 (s, 2H), 0.88 (s, 6H). ^{13}C NMR (101 MHz, DMSO-d6) δ 165.39, 162.08, 161.66, 159.94, 151.84, 148.66, 138.26, 138.09, 137.61, 135.18, 134.90, 132.69, 130.48, 129.96, 128.25, 124.25, 117.82, 117.37, 107.99, 50.60, 45.89, 35.43, 25.92, 22.74, 18.13. HRMS (ESI, *m*/*z*) $[M+H]^+$ calcd for $C_{29}H_{33}N_6O$: 481.2716, found: 481.2719.

*4.1.7.3. 4-(((2-(Diethylamino)ethyl)amino)methyl)-N-(4-methyl-3-((4-(pyridin-3-yl)pyrimidin-2-yl)amino)phenyl)benzamide(**14c**).* Yield 79%. ^{1}H NMR (400 MHz, DMSO-d6) δ 10.22 (s, 1H), 9.28 (s, 1H), 8.98 (s, 1H), 8.70 (s, 1H), 8.51 (s, 2H), 8.10 (s, 1H), 7.98 (s, 2H), 7.58–7.44 (m, 5H), 7.23 (s, 1H), 3.95 (s, 2H), 2.78 (s, 8H), 2.23 (s, 4H), 1.07 (s, 6H). ^{13}C NMR (101 MHz, DMSO-d6) δ 165.61, 162.08, 161.68, 159.93, 151.83, 148.67, 142.83, 138.26, 137.72, 134.91, 134.23, 132.70, 130.46, 128.72, 128.15, 128.08, 124.24, 117.81, 117.35, 107.98, 52.21, 51.11, 47.00, 45.30, 18.14, 11.19. HRMS (ESI, *m*/*z*) $[M+H]^+$ calcd for $C_{30}H_{36}N_7O$: 510.2981, found: 510.2986.

*4.1.7.4. N-(4-Methyl-3-((4-(pyridin-3-yl)pyrimidin-2-yl)amino) phenyl)-4-(((2-(pyrrolidin-1-yl)ethyl)amino)methyl)benzamide (**14d**).* Yield 78%. ^{1}H NMR (400 MHz, DMSO-d6) δ 10.22 (s, 1H), 9.29 (s, 1H), 8.98 (s, 1H), 8.69 (s, 1H), 8.52 (s, 2H), 8.11 (s, 1H), 7.97 (s, 2H), 7.72–7.31 (m, 5H), 7.22 (s, 1H), 3.93 (s, 2H), 2.86 (s, 8H), 2.24 (s, 3H), 1.83 (s, 4H). ^{13}C NMR (101 MHz, DMSO-d6) δ 165.56, 162.08, 161.67, 159.95, 151.85, 148.67, 142.31, 138.25, 137.67, 134.90, 134.33, 132.69, 130.47, 128.85, 128.13, 124.25, 117.79, 117.32, 107.99, 53.73, 53.58, 51.87, 45.16, 23.30, 18.12. HRMS (ESI, *m*/*z*) $[M+H]^+$ calcd for $C_{30}H_{34}N_7O$: 508.2825, found: 508.2829.

*4.1.7.5. 4-(((2-Hydroxyethyl)amino)methyl)-N-(4-methyl-3-((4-(pyridin-3-yl)pyrimidin-2-yl)amino)phenyl)benzamide (**14e**).* Yield 83%. ^{1}H NMR (400 MHz, DMSO-d6) δ 10.19 (s, 1H), 9.29 (s, 1H), 8.98 (s, 1H), 8.69 (s, 1H), 8.52 (s, 2H), 8.11 (s, 1H), 7.95 (s, 2H), 7.52–7.43 (m, 5H), 7.22 (s, 1H), 4.69 (s, 1H), 3.91 (s, 2H), 3.54 (s, 2H), 2.69 (s, 2H), 2.24 (s, 3H). ^{13}C NMR (101 MHz, DMSO-d6) δ 165.80, 162.09, 161.66, 159.92, 151.82, 148.65, 145.23, 138.28, 137.71, 134.90, 133.79, 132.69, 130.52, 128.22, 128.01, 124.24, 117.69, 117.27, 108.00, 60.85, 52.96, 51.49, 18.11, −15.38. HRMS (ESI, *m*/*z*) $[M+H]^+$ calcd for $C_{26}H_{27}N_6O_2$: 455.2195, found: 455.2191.

*4.1.8. Compounds **15a-r** were prepared following the synthetic procedure of **13a***

*4.1.8.1. 4-((N-(2-(Dimethylamino)ethyl)acrylamido)methyl)-N-(4-methyl-3-((4-(pyridin-3-yl)pyrimidin-2-yl)amino)phenyl)benzamide (**15a**).* Yield 67%. ^{1}H NMR (400 MHz, DMSO-d6) δ 10.23 (s, 1H), 9.27 (s, 1H), 9.00 (s, 1H), 8.68 (d, *J* = 3.3 Hz, 1H), 8.14–7.85 (m, 3H), 7.54–7.29 (m, 5H), 7.20 (d, *J* = 8.3 Hz, 1H), 6.73 (dd, *J* = 16.5, 10.3 Hz, 1H), 6.23 (dd, *J* = 16.8, 10.6 Hz, 1H), 5.80–5.70 (m, 1H), 4.83 (s, 1H), 4.67 (s, 1H), 3.67 (s, 2H), 3.14 (s, 2H), 2.69 (s, 6H), 2.22 (s, 3H). HRMS (ESI, *m*/*z*) $[M+H]^+$ calcd for $C_{31}H_{34}N_7O_2$: 536.2774, found: 536.2771.

*4.1.8.2. 4-((N-(2-(Dimethylamino)ethyl)propionamido)methyl)-N-(4-methyl-3-((4-(pyridin-3-yl)pyrimidin-2-yl)amino)phenyl)benzamide (**15b**).* Yield 56%. ^{1}H NMR (400 MHz, DMSO-d6) δ 10.20 (s, 1H), 9.29 (s, 1H), 9.00 (s, 1H), 8.69 (s, 1H), 8.52–8.48 (m, 2H), 8.09 (s, 1H), 7.99–7.91 (m, 2H), 7.54–7.37 (m, 5H), 7.22 (d, *J* = 8.4 Hz, 1H), 4.70 (s, 1H), 4.63 (s, 1H), 3.50–3.30 (m, 4H), 2.69–2.24 (m, 11H), 1.06–0.98 (m, 3H). ^{13}C NMR (101 MHz, DMSO-d6) δ 174.78, 165.56, 162.07, 161.63, 159.93, 151.80, 148.61, 141.47, 138.24, 137.64, 134.92, 132.68, 130.45, 128.71, 128.34, 127.87, 126.83, 124.26, 117.78, 117.39, 108.01, 54.16, 53.78, 50.45, 42.97, 42.06, 41.15, 26.14, 18.10, 12.56, 9.61. HRMS (ESI, *m*/*z*) $[M+H]^+$ calcd for $C_{31}H_{36}N_7O_2$: 538.2930, found: 538.2936.

*4.1.8.3. (E)-4-((N-(2-(Dimethylamino)ethyl)but-2-enamido)methyl)-N-(4-methyl-3-((4-(pyridin-3-yl)pyrimidin-2-yl)amino)phenyl)benzamide (**15c**).* Yield 76%.^{1}H NMR (400 MHz, DMSO-d6) δ 10.22 (s, 1H), 9.29 (s, 1H), 8.99 (s, 1H), 8.70 (s, 1H), 8.50 (d, *J* = 7.6 Hz, 2H), 8.10–7.99 (m, 3H), 7.61–7.27 (m, 5H), 7.22 (s, 1H), 6.83 (s, 1H), 6.46 (d, *J* = 7.3 Hz, 1H), 4.74 (s, 2H), 3.68 (s, 2H), 3.19 (s, 2H), 2.76 (s, 6H), 2.24 (s, 3H), 1.87 (s, 3H). ^{13}C NMR (101 MHz, DMSO-d6) δ 165.58, 162.07, 161.68, 159.94, 151.86, 148.68, 142.32, 138.29, 137.61, 134.90,

132.70, 130.49, 128.57, 128.32, 127.89, 126.93, 124.26, 122.28, 117.76, 117.27, 108.02, 55.40, 50.68, 44.60, 44.14, 18.29, 18.10. HRMS (ESI, *m/z*) $[M+H]^+$ calcd for $C_{32}H_{36}N_7O_2$: 550.2930, found: 550.2930.

*4.1.8.4. 4-((N-(2-(Dimethylamino)ethyl)cyclopropanecarboxamido) methyl)-N-(4-methyl-3-((4-(pyridin-3-yl)pyrimidin-2-yl)amino) phenyl)benzamide (**15d**).* Yield 72%. ^{1}H NMR (400 MHz, DMSO-d6) δ 10.20 (s, 1H), 9.27 (s, 1H), 8.98 (s, 1H), 8.68 (s, 1H), 8.49 (dd, $J = 8.9$, 7.0 Hz, 2H), 8.14–7.84 (m, 3H), 7.50–7.34 (m, 5H), 7.21 (d, $J = 6.6$ Hz, 1H), 4.89 (s, 1H), 4.61 (s, 1H), 3.58 (s, 2H), 2.85–2.36 (m, 8H), 2.22 (s, 3H), 2.01–1.88 (m, 1H), 0.69–0.79 (m, 4H). ^{13}C NMR (101 MHz, DMSO-d6) δ 173.24, 165.65, 162.08, 161.67, 159.91, 151.84, 148.66, 142.62, 138.28, 137.64, 134.85, 132.69, 130.50, 128.49, 128.28, 127.76, 126.92, 124.24, 117.71, 117.26, 107.99, 58.07, 56.70, 51.13, 49.16, 45.64, 45.23, 44.03, 18.12, 11.22, 8.07. HRMS (ESI, *m/z*) $[M+H]^+$ calcd for $C_{32}H_{36}N_7O_2$: 550.2930, found: 550.2933.

*4.1.8.5. 4-((N-(2-(Dimethylamino)ethyl)isobutyramido)methyl)-N-(4-methyl-3-((4-(pyridin-3-yl)pyrimidin-2-yl)amino)phenyl)benzamide (**15e**).* Yield 69%. ^{1}H NMR (400 MHz, DMSO-d6) δ 10.23 (s, 1H), 9.28 (s, 1H), 8.98 (s, 1H), 8.69 (s, 1H), 8.50 (d, $J = 9.5$ Hz, 2H), 8.15–7.87 (m, 3H), 7.59–7.15 (m, 6H), 4.78 (s, 1H), 4.60 (s, 1H), 3.63 (s, 2H), 3.18 (s, 2H), 2.76 (s, 7H), 2.23 (s, 3H), 1.05 (s, 6H). ^{13}C NMR (101 MHz, DMSO-d6) δ 177.85, 177.08, 165.48, 162.06, 161.65, 159.94, 151.83, 148.64, 141.81, 138.24, 137.64, 134.91, 134.54, 132.69, 130.47, 128.65, 128.32, 127.66, 126.73, 124.25, 117.75, 117.32, 108.00, 54.29, 50.81, 43.62, 43.21, 41.92, 30.11, 29.66, 20.33, 20.09, 18.12. HRMS (ESI, *m/z*) $[M+H]^+$ calcd for $C_{32}H_{38}N_7O_2$: 552.3087, found: 552.3081.

*4.1.8.6. 4-((N-(2-(Dimethylamino)ethyl)butyramido)methyl)-N-(4-methyl-3-((4-(pyridin-3-yl)pyrimidin-2-yl)amino)phenyl)benzamide (**15f**).* Yield 73%. ^{1}H NMR (400 MHz, DMSO-d6) δ 10.23 (s, 1H), 9.29 (s, 1H), 8.99 (s, 1H), 8.70 (s, 1H), 8.55–8.40 (m, 2H), 8.14–7.87 (m, 3H), 7.52–7.22 (m, 6H), 4.67 (s, 2H), 3.63 (s, 2H), 3.17 (s, 2H), 2.72 (s, 6H), 2.32–2.24 (m, 4H), 1.58–1.53 (m, 2H), 0.94–0.85 (m, 3H). ^{13}C NMR (101 MHz, DMSO-d6) δ 172.74, 165.61, 162.07, 161.66, 159.90, 151.83, 148.68, 142.68, 138.23, 137.65, 134.86, 132.66, 130.51, 128.51, 128.21, 127.64, 126.76, 124.22, 117.69, 117.22, 107.99, 57.94, 56.88, 51.07, 48.47, 45.75, 45.48, 43.70, 34.66, 34.25, 18.76, 18.08, 14.24. HRMS (ESI, *m/z*) $[M+H]^+$ calcd for $C_{32}H_{38}N_7O_2$: 552.3087, found: 552.3089.

*4.1.8.7. 4-((N-(2-(Dimethylamino)ethyl)pivalamido)methyl)-N-(4-methyl-3-((4-(pyridin-3-yl)pyrimidin-2-yl)amino)phenyl)benzamide (**15g**).* Yield 81%. ^{1}H NMR (400 MHz, DMSO-d6) δ 10.23 (s, 1H), 9.29 (s, 1H), 8.99 (s, 1H), 8.70 (s, 1H), 8.59–8.38 (m, 2H), 8.10–7.98 (m, 3H), 7.52–7.22 (m, 6H), 4.86 (s, 2H), 3.52 (s, 2H), 3.16 (s, 2H), 2.73 (s, 6H), 2.24 (s, 3H), 1.25 (s, 9H). ^{13}C NMR (101 MHz, DMSO-d6) δ 177.32, 165.62, 161.64, 159.92, 151.81, 148.66, 142.19, 138.26, 137.65, 134.92, 134.29, 132.67, 130.49, 128.41, 127.02, 124.26, 117.73, 117.28, 107.99, 56.15, 51.02, 44.84, 28.72, 18.11. HRMS (ESI, *m/z*) $[M+H]^+$ calcd for $C_{33}H_{40}N_7O_2$: 566.3243, found: 566.3246.

*4.1.8.8. 4-((2-(Dimethylamino)-N-(2-(dimethylamino)ethyl)acetamido)methyl)-N-(4-methyl-3-((4-(pyridin-3-yl)pyrimidin-2-yl) amino)phenyl)benzamide (**15h**).* Yield 76%. ^{1}H NMR (400 MHz, DMSO-d6) δ 10.27 (s, 1H), 9.29 (s, 1H), 9.00 (s, 1H), 8.69 (s, 1H), 8.50–8.48 (m, 2H), 8.35–8.25 (m, 1H), 8.16–7.89 (m, 3H), 7.73 (s, 1H), 7.53–7.44 (m, 4H), 7.23 (s, 1H), 4.67 (s, 2H), 4.01–2.99 (m, 6H), 2.67–2.25 (m, 15H). ^{13}C NMR (101 MHz, DMSO-d6) δ 168.13, 167.68, 165.44, 162.06, 161.64, 159.94, 151.82, 148.63, 141.37, 140.33, 138.22, 137.63, 134.91, 134.70, 134.39, 132.67, 130.46, 128.71, 128.41, 128.14, 127.88, 127.52, 124.25, 117.84, 117.40, 107.99, 59.32, 53.67, 44.79, 44.67, 43.72, 43.35, 18.13. HRMS (ESI, *m/z*) $[M+H]^+$ calcd for $C_{32}H_{39}N_8O_2$: 567.3196, found: 567.3199.

*4.1.8.9. N-(2-(Dimethylamino)ethyl)-N-(4-((4-methyl-3-((4-(pyridin-3-yl)pyrimidin-2-yl)amino)phenyl)carbamoyl)benzyl)nicotinamide (**15i**).* Yield 63%. ^{1}H NMR (400 MHz, DMSO-d6) δ 10.21 (s, 1H), 9.29 (s, 1H), 8.98 (s, 1H), 8.69–8.49 (m, 5H), 8.10–7.83 (m, 4H), 7.63–7.29 (m, 6H), 7.23 (s, 1H), 4.82 (s, 1H), 4.63 (s, 1H), 3.50 (s, 1H), 3.27 (s, 1H), 2.34–1.93 (m, 11H). ^{13}C NMR (101 MHz, DMSO-d6) δ 170.24, 165.46, 162.05, 161.62, 159.95, 151.82, 150.99, 148.60, 147.77, 140.43, 138.21, 137.61, 135.10, 134.93, 132.67, 132.19, 130.47, 128.69, 128.18, 127.14, 124.28, 123.85, 117.82, 117.40, 108.01, 53.72, 53.58, 52.18, 42.90, 18.11. HRMS (ESI, *m/z*) $[M+H]^+$ calcd for $C_{34}H_{35}N_8O_2$: 587.2883, found: 587.2888.

*4.1.8.10. N-(2-(Dimethylamino)ethyl)-N-(4-((4-methyl-3-((4-(pyridin-3-yl)pyrimidin-2-yl)amino)phenyl)carbamoyl)benzyl)isoxazole-5-carboxamide (**15j**).* Yield 67%. ^{1}H NMR (400 MHz, DMSO-d6) δ 10.20 (s, 1H), 9.27 (s, 1H), 8.98 (s, 1H), 8.68 (s, 2H), 8.50 (s, 2H), 8.08 (s, 1H), 7.94 (s, 2H), 7.52–7.42 (m, 5H), 7.25–6.84 (m, 2H), 4.80 (s, 2H), 3.49 (s, 2H), 2.68–2.05 (m, 11H). HRMS (ESI, *m/z*) $[M+H]^+$ calcd for $C_{32}H_{33}N_8O_3$: 577.2676, found: 577.2675.

*4.1.8.11. N-(2-(Dimethylamino)ethyl)-N-(4-((4-methyl-3-((4-(pyridin-3-yl)pyrimidin-2-yl)amino)phenyl)carbamoyl)benzyl)thiophene-2-carboxamide (**15k**).* Yield 63%. ^{1}H NMR (400 MHz, DMSO-d6) δ 10.25 (s, 1H), 9.30 (s, 1H), 9.01 (s, 1H), 8.71 (s, 1H), 8.52 (dd, $J = 12.1$, 4.8 Hz, 2H), 8.33–7.76 (m, 4H), 7.74–7.32 (m, 7H), 7.32–7.16 (m, 2H), 4.79 (s, 2H), 3.68 (s, 2H), 3.09 (s, 4H), 2.75 (s, 4H), 2.25 (s, 3H). HRMS (ESI, *m/z*) $[M+H]^+$ calcd for $C_{33}H_{34}N_7O_2S$: 592.2495, found: 592.2496.

*4.1.8.12. N-(2-(Dimethylamino)ethyl)-4-methyl-N-(4-((4-methyl-3-((4-(pyridin-3-yl)pyrimidin-2-yl)amino)phenyl)carbamoyl)benzyl) benzamide (**15l**).* Yield 66%. ^{1}H NMR (400 MHz, DMSO-d6) δ 10.22 (s, 1H), 9.27 (s, 1H), 8.98 (s, 1H), 8.68 (s, 1H), 8.50 (s, 2H), 8.08 (s, 1H), 7.95 (s, 2H), 7.50–7.22 (m, 11H), 4.69 (s, 2H), 3.58 (s, 1H), 2.95 (s, 1H), 2.32–2.04 (s, 11H). HRMS (ESI, *m/z*) $[M+H]^+$ calcd for $C_{36}H_{38}N_7O_2$: 600.3087, found: 600.3092.

*4.1.8.13. 4-((N-(2-(Diethylamino)ethyl)acrylamido)methyl)-N-(4-methyl-3-((4-(pyridin-3-yl)pyrimidin-2-yl)amino)phenyl)benzamide (**15m**).* Yield 71%. ^{1}H NMR (400 MHz, DMSO-d6) δ 10.25 (s, 1H), 9.31 (d, $J = 8.0$ Hz, 1H), 9.01 (d, $J = 8.7$ Hz, 1H), 8.72 (d, $J = 4.4$ Hz, 1H), 8.63–8.40 (m, 2H), 8.33–7.84 (m, 4H), 7.75–7.29 (m, 6H), 7.31–7.11 (m, 1H), 6.90–6.76 (m, 1H), 6.42–6.14 (m, 1H), 5.91–5.61 (m, 1H), 4.89 (s, 1H), 4.74 (s, 1H), 3.62–2.24 (m, 11H), 1.14 (s, 6H). HRMS (ESI, *m/z*) $[M+H]^+$ calcd for $C_{33}H_{38}N_7O_2$: 564.3087, found: 564.3086.

4.1.8.14. N-(2-(Diethylamino)ethyl)-N-(4-((4-methyl-3-((4-(pyridin-3-yl)pyrimidin-2-yl)amino)phenyl)carbamoyl)benzyl)nicotinamide (15n). Yield 75%. ^{1}H NMR (400 MHz, DMSO-d6) δ 10.25 (s, 2H), 9.32 (d, $J = 3.1$ Hz, 1H), 9.02 (s, 1H), 8.82–8.47 (m, 5H), 8.10 (s, 1H), 8.06–7.89 (m, 3H), 7.66–7.31 (m, 6H), 7.23 (s, 1H), 4.67 (s, 2H), 3.78–2.93 (m, 8H), 2.24 (s, 3H), 1.25 (s, 6H). ^{13}C NMR (101 MHz, DMSO-d6) δ 170.08, 165.44, 162.09, 161.65, 159.94, 153.55, 151.82, 151.11, 150.70, 148.65, 147.65, 140.59, 138.29, 137.62, 134.92, 132.71, 132.07, 130.54, 128.68, 128.16, 127.20, 124.26, 123.93, 117.74, 117.34, 108.02, 52.76, 47.69, 47.12, 18.12, 8.98. HRMS (ESI, *m/z*) $[M+H]^+$ calcd for $C_{36}H_{39}N_8O_2$: 615.3196, found: 615.3199.

*4.1.8.15. N-(4-((4-Methyl-3-((4-(pyridin-3-yl)pyrimidin-2-yl)amino) phenyl)carbamoyl)benzyl)-N-(2-(pyrrolidin-1-yl)ethyl)nicotinamide (**15o**).* Yield 86%. ^{1}H NMR (400 MHz, DMSO-d6) δ 10.55 (s, 1H), 10.24 (s, 1H), 9.33 (s, 1H), 9.04 (s, 1H), 8.83–8.51 (m, 5H), 8.19–7.90 (m, 4H), 7.65 (s, 1H), 7.48–7.22 (m, 5H), 4.68 (s, 2H), 3.78–2.74 (m,

8H), 2.24 (s, 3H), 2.02 (s, 2H), 1.92 (s, 2H). HRMS (ESI, *m/z*) $[M+H]^+$ calcd for $C_{36}H_{37}N_8O_2$: 613.3039, found: 613.3036.

*4.1.8.16. 4-((N-Isopentylacrylamido)methyl)-N-(4-methyl-3-((4-(pyridin-3-yl)pyrimidin-2-yl)amino)phenyl)benzamide (**15p**).* Yield 71%. ^{1}H NMR (400 MHz, DMSO-d6) δ 10.17 (s, 1H), 9.27 (s, 1H), 8.96 (s, 1H), 8.68 (s, 1H), 8.56–8.35 (m, 2H), 8.08 (s, 1H), 7.92 (d, J = 8.1 Hz, 2H), 7.41 (ddd, J = 26.6, 20.0, 8.7 Hz, 5H), 7.20 (d, J = 6.8 Hz, 1H), 6.89–6.61 (m, 1H), 6.20 (t, J = 15.6 Hz, 1H), 5.70 (dd, J = 42.6, 9.8 Hz, 1H), 4.70 (d, J = 43.9 Hz, 1H), 4.64 (s, 1H), 2.22 (s, 3H), 1.51–1.23 (m, 5H), 0.85 (s, 6H). HRMS (ESI, *m/z*) $[M+H]^+$ calcd for $C_{32}H_{35}N_6O_2$: 535.2821, found: 535.2824.

*4.1.8.17. N-(2-Hydroxyethyl)-N-(4-((4-methyl-3-((4-(pyridin-3-yl)pyrimidin-2-yl)amino)phenyl)carbamoyl)benzyl)nicotinamide (**15q**).* Yield 75%.^{1}H NMR (400 MHz, DMSO-d6) δ 10.22 (s, 1H), 9.29 (s, 1H), 8.99 (s, 1H), 8.70–8.65 (m, 3H), 8.52 (s, 2H), 8.10 (s, 1H), 7.96 (s, 3H), 7.56–7.28 (m, 6H), 7.22 (s, 1H), 4.87 (s, 2H), 4.65 (s, 1H), 3.65 (s, 1H), 3.49 (s, 2H), 3.27 (s, 1H), 2.24 (s, 3H). HRMS (ESI, *m/z*) $[M+H]^+$ calcd for $C_{32}H_{30}N_7O_3$: 560.2410, found: 560.2416.

*4.1.8.18. 4-((2-(Dimethylamino)-N-(2-hydroxyethyl)acetamido)methyl)-N-(4-methyl-3-((4-(pyridin-3-yl)pyrimidin-2-yl)amino)phenyl)benzamide (**15r**).* Yield 62%.^{1}H NMR (400 MHz, DMSO-d6) δ 10.22 (s, 1H), 9.28 (s, 1H), 8.99 (s, 1H), 8.69 (s, 1H), 8.52 (s, 2H), 8.09–7.95 (m, 3H), 7.51–7.43 (m, 5H), 7.22 (s, 1H), 4.70 (s, 2H), 4.30 (s, 1H), 3.58 (s, 2H), 3.30 (s, 2H), 2.73 (s, 6H), 2.23 (s, 3H). HRMS (ESI, *m/z*) $[M+H]^+$ calcd for $C_{30}H_{34}N_7O_3$: 540.2723, found: 540.2726.

4.2. Biology

4.2.1. BaF3 isogenic cell generation

Retroviral constructs for BaF3-KIT mutants were made based on the pMSCVpuro (Clontech) backbone. For TEL-KIT vector, the first 1 kb of human TEL gene with an artificial myristoylation sequence (MGCGCSSHPEDD) was cloned into the pMSCVpuro retroviral vector, followed by a 3xFLAG tag sequence and a stop codon. Then, the kinase domain coding sequence of KIT was inserted in-frame between TEL and 3xFLAG sequences. For full-length expression vectors, the coding sequences of KIT variants were directly cloned in pMSCVpuro vector with a 3xFLAG tag at the C-terminal end. All mutagenesis were performed using the QuikChange Site-Directed Mutagenesis Kit (Stratagene) following the manufacturer's instructions. Retrovirus was packaged in HEK293T cells by transfecting KIT-containing MSCV vectors together with two helper plasmids. Virus supernatants were harvested 48 h after transfection and filtered before infection. Then BaF3 cells were infected with harvested virus supernatants using spinoculation protocol and stable cell lines were obtained by puromycin selection for 48 h. The IL-3 concentrations in the culture medium were gradually withdrawn until cells were able to grow in the absence of IL-3. TEL-PDGFRα BaF3, TEL-PDGFRβBaF3, TEL-VEGFR2 BaF3 cells were generated following the same procedure of TEL-c-KITBaF3 using different kinase domain coding sequences.

4.2.2. Cell lines and cell culture

EOL-1 cell line was obtained from Deutsche Sammlung von Mikroorganismen und Zellkulturen GmbH (DSMZ) and NCI-H1703 cell line was obtained from American Type Culture Collection (Manassas, VA). All the cells were grown in a humidified incubator (Thermo, USA) at 37 °C under 5% CO_2. EOL-1, NCI-H1703 cell lines and all the isogenic BaF3 cells were grown in RPMI 1640 medium supported with 10% FBS, and 1% penicillin/streptomycin. Adherent cells were grown in tissue culture flasks until they were 85–95% confluent prior to use. For suspension cells, cells were collected by spin down at 700 rpm/min for 4 min before use.

4.2.3. Cloning, expression, and purification of PDGFRα

Constructs spanning residues 550–973 with the deletion of residues 697–768 of the human PDGFRα were expressed and purified using a baculovirus/insect cell system as described previously [22]. DNA encoding the human PDGFRα kinase domain (residues 550–973) was obtained from the cDNA of BT549 and cloned into the pFastBac™ HTA vector (Invitrogen) to acquire a fusion with six-His tag and a TEV protease cleavage site at the N-terminus. Transfection, virus generation, virus amplification and expression were carried out in SF9 cells using the Bac-to-Bac Baculovirus expression system (Invitrogen). Cells pellets were suspended into lysis buffer containing 20 mM Tris-HCl (pH 8.0), 5 mM KCl, 150 mM NaCl, 1% Glycerol, 20 mM imidazole, 1 mM tris (2-carboxyethyl) phosphine hydrochloride (TCEP), and protease inhibitor mixture (Complete EDTA-free, Roche). The lysate was centrifuged with 20,000 rpm for 1 h at 4 °C, then the supernatant was incubated with Ni-NTA Sepharose beads (GE). The N-terminal six-His tag was removed by incubation with TEV for 4 h at 4 °C. The cleaved protein was further purified by size exclusion chromatography (Superdex 200) in the buffer containing 20 mM Tris-HCl pH8.0, 150 mM NaCl, 1% Glycerol, 1 mM TCEP and was concentrated to 20 mg/mL, and aliquots were flash frozen in liquid nitrogen for storage at −80 °C.

4.2.4. Kinase biochemical assay

The ADP-Glo™ kinase assay (Promega, Madison, WI) was used to screen compound **15i** for its PDGFRα/β, c-Kit inhibition effects. The kinase reaction system contains 9 μL PDGFRα/β, c-Kit (10 ng/μL), 1 μL of serially diluted compound **15i**, and 10 μL substrate Poly (4:1 Glu, Tyr) peptide (0.4 μg/μL) (Promega, Madison, WI) with 100 μM ATP (Promega, Madison, WI). The reaction in each tube was started immediately by adding ATP and kept going for an hour under 37 °C. After the tube was cooled for 5 min at room temperature, 5 μL solvent reactions were carried out in a 384-well plate. Then 5 μL of ADP-Glo™ reagent was added into each well to stop the reaction and consume the remaining ATP within 40 min. At the end, 10 μL of kinase detection reagent was added into the well and incubated for 30 min to produce a luminescence signal. The luminescence signal was measured with an automated plate reader (Envision, PE, USA) and the dose-response curve was fitted using Prism 5.0 (GraphPad Software Inc., San Diego, CA).

4.2.5. General procedure for anti-proliferation assays

A density of $1–3 \times 10^4$ cells/mL cells were mixed with various concentrations of compounds then 100 μL suspension was added to each well and incubated for 72 h. Cell viability was determined using the CellTiter-Glo (Promega, USA) or CCK-8 (Beboy, China). Both assays were performed according to the manufacturer instructions. For CellTiter-Glo assay, luminescence was determined in a multi-label reader (Envision, PerkinElmer, USA). For CCK-8 assay, absorbance was measured in a microplate reader (iMARK, Bio-Rad, USA) at 450 nm and 655 nm. Data were normalized to control group (DMSO). GI_{50} values were calculated using Prism 5.0 (GraphPad Software, San Diego, CA). To compare the significance of tested compounds with imatinib, using One-way ANOVA (and nonparametric) method of column analyses in Prism 5.0 (GraphPad Software, San Diego, CA), the p-values were calculated by using imatinib as the reference compound.

4.2.6. Signaling pathway study

EOL-1, NCI-H1703 cells were treated with DMSO, serially diluted compound **15i** and 1 μM imatinib for 2 h. Cells were then washed with cold PBS and lysed in RIPA buffer (Beyotime, China). Western blotting was performed by standard methods, as previously

described. The following antibodies were used at a range of antibody concentrations as indicated by the manufacturers to probe for specific proteins: Polyclonal rabbit antibodies to total p42/44 mitogen activated protein kinase (MAPK) (cat.no.4695), phospho-p44/42 MAPK T202/Y204 (cat.no.4370), phospho-AKT S473 (cat.no.4060), total AKT (cat.no.4691), phospho-Stat5 (cat.no.9314), total Stat5 (cat.no.9363), phospho-Stat3 (cat.no.9145), total Stat3 (cat.no.12640), phospho-PDGFRα Y1018 (cat.no.4547), phospho-PDGFRα Y754(cat.no.2992), phospho-PDGFRα Y849/PDGFRβ Y857 (cat.no.3170), total PDGFRα (cat.no.3174) were from Cell Signaling Technology. Beta Actin antibodies were purchased from Sigma (cat.no.A5316).

4.2.7. Apoptosis effect examination

EOL-1, NCI-H1703 cells were treated with DMSO, specified concentrations of compound **15i** and imatinib for the indicated periods. Cells were collected and analyzed by Western blotting using the following antibodies: PARP (cat.no.9532), Caspase-3 (cat.no.9665) from Cell Signaling Technology. Beta Actin antibodies were purchased from Sigma (cat. no. A5316).

4.2.8. Cell cycle analysis

EOL-1, NCI-H1703 cells were treated with DMSO, specified concentrations of compound **15i** and imatinib for the indicated periods. Cells were fixed in 70% cold ethanol and incubated at −20 °C overnight then stained with PI/RNase staining buffer (BD Pharmingen). Flow cytometry was performed using a FACS Calibur (BD), and results were analyzed by ModFit software.

4.2.9. In vivo pharmacokinetics study

Compound **15i** was dissolved in 55% saline containing 5% DMSO and 40% PEG400 by vortex. The final concentration of the stock solution was 1 mg/mL for administration. Six-eight weeks old male Sprague-Dawely rats were fasted overnight before starting drug treatment via intravenous and oral administration. Animal blood collection time points were as follows: for group 1, 3, 5 (intravenous): 1 min, 5 min, 15 min, 30 min, 1 h, 2 h, 4 h, 6 h, 8 h before and after administration was selected; for group 2, 4, 6 (oral): 5 min, 15 min, 30 min, 1 h, 2 h, 4 h, 6 h, 8 h and 24 h before and after dosing. Each time about 0.2 mL blood was collected through the jugular vein adding heparin for anticoagulation and kept on ice. Then plasma was separated by centrifugation at 8000 rpm for 6 min at 2–8 °C. The obtained plasma was stored at −80 °C before analysis. After finishing the test, all surviving animals will be transferred to the repository or euthanasia (CO_2 asphyxiation).

4.2.10. EOL-1 xenograft tumor model

Six weeks old female nu/nu mice were purchased from the Shanghai Experimental Center, Chinese Academy of Sciences (Shanghai, China). All animals were maintained in a specific pathogen-free facility and used according to the animal care regulations of Hefei Institutes of Physical Science, Chinese Academy of Sciences (Hefei, China), and all efforts were made to minimize animal suffering. To obtain orthotopic xenograft of human mammary tumor in the mice, cells were harvested during exponential growth. Five million EOL-1 cells in PBS were suspended in a 1:1 mixture with Matrigel (BD Biosciences) and injected into the subcutaneous space on the right flank of nu/nu mice. Daily IP injection was initiated when EOL-1 tumors had reached a size of 200–400 mm^3. Animals were then randomized into treatment groups of 6 mice each for efficacy studies. Compound **15**i and imatinib was delivered daily in a HKI solution (0.5% Methocellulose/0.4% Tween80 in ddH_2O) by IP injection. A range of doses of **15i** and imatinib or its vehicle was administered, as indicated in Fig. 8 legends. Body weight and tumor growth was measured daily after **15i** and imatinib treatments. Tumor volumes were calculated as follows: tumor volume (mm^3) = [($W^2 \times L$)/2] in which width (W) is defined as the smaller of the two measurements and length (L) is defined as the larger of the two measurements.

4.2.11. HE staining

HE staining was carried out according to the previous report. First hydrate the sections and then dip the slide into a Coplin jar containing Mayer's hematoxylin and agitate for 30 s. After rinsing the slide in H_2O for 1 min, stain with 1% eosin Y solution for 10–30 s with agitation. Subsequently, dehydrate the sections with two changes of 95% alcohol and two changes of 100% alcohol for 30 s each. And then extract the alcohol with two changes of xylene. Finally, add one or two drops of mounting medium and cover with a cover slip.

4.2.12. Ki-67 staining

For IHC demonstration of Ki-67, tissue sections were quenched for endogenous peroxides and placed in an antigen retrieval solution (0.01 M citrate buffer, pH 6.0) for 15 min in a microwave oven at 100 °C at 600 W. After incubation in the casein block, mouse MAb anti-Ki-67 (ZSGB-BIO, China) was applied to the sections at dilutions of 1:50. Incubations with primary antibodies lasted overnight at 4 °C. The secondary detection system was used to visualize antibody binding. Staining was developed with DAB, and the slides were counterstained with hematoxylin, dehydrated and mounted.

4.2.13. TUNEL staining

TUNEL staining was performed using the POD in Situ Cell Death Detection kit (Roche, USA). Briefly, sections were deparaffinized in xylene, rehydrated in decreasing concentration of ethanol, and then treated by nuclease free Proteinase K for 15 min at room temperature before endogenous peroxidase was blocked in 3% H_2O_2 in methanol. Terminal deoxynucleotidyl transferase (TdT) in reaction buffer was applied to sections for 1 h at 37 °C. Following washes, the slides were covered by converter-POD solution for 30 min at 37 °C. Apoptotic cells were detected after incubation in 3, 3′-diaminobenzidine (DAB) chromogen (Beyotime Biotechnology, China) for approximately 8 min and the slides were counterstained with hematoxylin.

4.2.14. EOL-1 engraftment tumor model

Five weeks old female NOD-SCID mice were purchased from the Shanghai Experimental Center, Chinese Science Academy (Shanghai, China). All animals were housed in a specific pathogen-free facility and used according to the animal care regulations of Hefei Institutes of Physical Science, Chinese Academy of Sciences. NOD-SCID mice were irradiated (2 Gy) 24 h before tail vein injection of 5 million EOL-1 cells in 0.3 mL 1640.**15i** or imatinib treatments were initiated daily by i.p. 3 weeks after cell inoculation. Mice were monitored daily and were euthanized when moribund or at early signs of hind limb paralysis.

4.2.15. FACS detection of drug efficacy

Single cell suspensions from bone marrow of EOL-1 engrafted NOD-SCID mice were prepared, and red blood cells were lysed. Single-cell suspensions were blocked and incubated with PE-conjugated HLA-ABC (G46–2.6). Samples were acquired by a BD FACScalibur cytometer and analyzed by FlowJo software. Appropriate isotype-matched, irrelevant control mAbs were used to determine the level of background staining. The antibodies were purchased from BD Biosciences (San Diego, USA).

4.2.16. Crystallization and structure determination

The crystals of PDGFRα in complex with **15i** were obtained by

sitting drop vapor diffusion in 0.2 M KCl, pH 7.0, and 20% PEG 3350 at 20 °C. For data collection, the crystals were rapidly dipped in reservoir solution supplemented with 25% ethylene glycol and were flash-frozen with liquid nitrogen. X-ray diffraction data were collected at beamline BL19U1 at Shanghai Synchrotron Radiation Facility (SSRF). The diffraction data were processed using HKL3000 [23]. The structure was determined by molecular replacement with Phaser [24] using FLT3 structure (PDB ID: 1RJB) [25] as a search model. Then multiple rounds of manual refitting and crystallographic refinement were performed using COOT [26] and Phenix [27]. Diffraction data, refinement statistics, PDB ID codes, and quality of the structure are summarized in Supplemental Table 2.

4.2.17. Homology modeling

The homology model of PDGFRβ was obtained by Modeller 9v18 [28] using the crystal structure of PDGFRα (PDB ID: 5GRN). The sequence alignment was performed automatically by MUSCLE [29]. 512 models of initial receptor were generated in Modeller with fully annealed protocol, and the optimal model was chosen according to DOPE score. To remove unfavorable steric contacts and to release strain among amino acid residues, the model was submitted to Prime (Schrodinger suite 2017) [30] for backbone-constrained truncated-Newton minimization refinement using the OPLS3 force field and implicit solvent model.

Notes

Dr. Shanchun Zhang is a shareholder of Hefei Cosource Medicine Technology Co. LTD.

Author contributions

The manuscript was written through contributions of all authors. All authors have given approval to the final version of the manuscript.

Acknowledgments

This work was supported by the National Natural Science Foundation of China (nos, 81602973, U1432250, U1532154, 31270769), the "Personalized Medicines——Molecular Signature-based Drug Discovery and Development", Strategic Priority Research Program of the Chinese Academy of Sciences (Grant No. XDA12020351), the Natural Science Foundation of Anhui Province (nos, 1708085QH197, 1608085QH180, 1708085MH208) and the Science and Technology Projects of Anhui Province (nos, 1501041175, 1704a0802140, 16030801114). We are also grateful for the National Program for Support of Top-Notch Young Professionals for J.L. and the “Hundred Talents Program” of CAS support for J.L. and W.W.

Appendix A. Supplementary data

Supplementary data related to this article can be found at https://doi.org/10.1016/j.ejmech.2018.03.003.

References

[1] P.H. Chen, X. Chen, X. He, Platelet-derived growth factors and their receptors: structural and functional perspectives, Biochim. Biophys. Acta 1834 (2013) 2176–2186.
[2] L. Terracio, C.H. Heldin, Induction of platelet-derived growth factor receptor expression in smooth muscle cells and fibroblasts upon tissue culturing, J. Cell Biol. 107 (1988) 1947–1957.
[3] R.H. Alvarez, H.M. Kantarjian, J.E. Cortes, R.H. Alvarez, H.M. Kantarjian, J.E. Cortes, Biology of platelet-derived growth factor and its involvement in disease, mayo, Clin. Proc. 81 (2006) 1241–1257.
[4] Y. Cao, Multifarious functions of PDGFs and PDGFRs in tumor growth and metastasis, Trends Mol. Med. 19 (2013) 460–473.
[5] R. Board, G.C. Jayson, Platelet-derived growth factor receptor (PDGFR): a target for anticancer therapeutics, Drug Resistance Updates : Reviews and Commentaries in Antimicrobial and Anticancer Chemotherapy 8 (2005) 75–83.
[6] J. Cools, H. Quentmeier, B.J. Huntly, P. Marynen, J.D. Griffin, H.G. Drexler, D.G. Gilliland, The EOL-1 cell line as an in vitro model for the study of FIP1L1-PDGFRA-positive chronic eosinophilic leukemia, Blood 103 (2004) 2802–2805.
[7] M.C. Heinrich, D.J. Griffith, B.J. Druker, C.L. Wait, K.A. Ott, A.J. Zigler, Inhibition of c-kit receptor tyrosine kinase activity by STI 571, a selective tyrosine kinase inhibitor, Blood 96 (2000) 925–932.
[8] E. Buchdunger, J. Zimmermann, H. Mett, T. Meyer, M. Müller, U. Regenass, N.B. Lydon, Selective inhibition of the platelet-derived growth factor signal transduction pathway by a protein-tyrosine kinase inhibitor of the 2-phenylaminopyrimidine class, Proc. Natl. Acad. Sci. U.S.A. 92 (1995) 2558–2562.
[9] L. Sun, C.S. Liang, Y. Zhou, T. Miller, J. Cui, J.Y. Fukuda, J.Y. Chu, A. Nematalla, X. Wang, H. Chen, Discovery of 5-(5-Fluoro-2-oxo-1,2- dihydroindol-(3Z)-ylidenemethyl)-2,4- dimethyl-1H-pyrrole-3-carboxylic acid (2-diethylaminoethyl)amide, a novel tyrosine kinase inhibitor targeting vascular endothelial and platelet-derived growth factor receptor T, J. Med. Chem. 46 (2003) 1116–1119.
[10] T. O'Hare, W.C. Shakespeare, X. Zhu, C.A. Eide, V.M. Rivera, F. Wang, L.T. Adrian, T. Zhou, W.S. Huang, Q. Xu, AP24534, a Pan-BCR-ABL inhibitor for chronic myeloid leukemia, potently inhibits the T315I mutant and overcomes mutation-based resistance, Canc. Cell 16 (2009) 401–412.
[11] D.D. Hu-Lowe, H.Y. Zou, M.L. Grazzini, M.E. Hallin, G.R. Wickman, K. Amundson, J.H. Chen, D.A. Rewolinski, S. Yamazaki, E.Y. Wu, M.A. McTigue, B.W. Murray, R.S. Kania, P. O'Connor, D.R. Shalinsky, S.L. Bender, Nonclinical antiangiogenesis and antitumor activities of axitinib (AG-013736), an oral, potent, and selective inhibitor of vascular endothelial growth factor receptor tyrosine kinases 1, 2, 3, Clin. Canc. Res. 14 (2008) 7272–7283.
[12] P. Dubreuil, S. Letard, M. Ciufolini, L. Gros, M. Humbert, N. Castéran, L. Borge, B. Hajem, A. Lermet, W. Sippl, Masitinib (AB1010), a potent and selective tyrosine kinase inhibitor targeting KIT, PLoS One 4 (2009) e7258–e7258.
[13] M.C. Heinrich, D. Griffith, A. Mckinley, J. Patterson, A. Presnell, A. Ramachandran, M. Debiecrychter, Crenolanib inhibits the drug-resistant PDGFRA D842V mutation associated with imatinib-resistant gastrointestinal stromal tumors, Clin. Canc. Res. 18 (2012) 4375–4384.
[14] F. Hilberg, G.J. Roth, M. Krssak, S. Kautschitsch, W. Sommergruber, U. Tontsch-Grunt, P. Garin-Chesa, G. Bader, A. Zoephel, J. Quant, A. Heckel, W.J. Rettig, BIBF 1120: triple angiokinase inhibitor with sustained receptor blockade and good antitumor efficacy, Canc. Res. 68 (2008) 4774–4782.
[15] D.H. Albert, P. Tapang, T.J. Magoc, L.J. Pease, D.R. Reuter, R.Q. Wei, J. Li, J. Guo, P.F. Bousquet, N.S. Ghoreishi-Haack, Preclinical activity of ABT-869, a multi-targeted receptor tyrosine kinase inhibitor, Mol. Canc. Therapeut. 5 (2006) 995–1006.
[16] D. Mahadevan, L. Cooke, C. Riley, R. Swart, B. Simons, C.K. Della, L. Wisner, M. Iorio, K. Shakalya, H. Garewal, A novel tyrosine kinase switch is a mechanism of imatinib resistance in gastrointestinal stromal tumors, Oncogene 26 (2007) 3909–3919.
[17] Y. Yarden, W.J. Kuang, T. Yang-Feng, L. Coussens, S. Munemitsu, T.J. Dull, E. Chen, J. Schlessinger, U. Francke, A. Ullrich, Human proto-oncogene c-kit: a new cell surface receptor tyrosine kinase for an unidentified ligand, EMBO J. 6 (1987) 3341–3351.
[18] Z. Zhao, H. Wu, L. Wang, Y. Liu, S. Knapp, Q. Liu, N.S. Gray, Exploration of type II binding mode: a PrivilegedApproach for kinase inhibitor focused drug discovery? ACS Chem. Biol. 9 (2014) 1230–1241.
[19] M.A. Fabian, B.W. Rd, D.K. Treiber, C.E. Atteridge, M.D. Azimioara, M.G. Benedetti, T.A. Carter, P. Ciceri, P.T. Edeen, M. Floyd, A small molecule-kinase interaction map for clinical kinase inhibitors, Nat. Biotechnol. 23 (2005) 329–336.
[20] J. Cools, E.H. Stover, C.L. Boulton, J. Gotlib, R.D. Legare, S.M. Amaral, D.P. Curley, N. Duclos, R. Rowan, J.L. Kutok, J. Cools, et al., PKC412 overcomes resistance to imatinib in a murine model of FIP1L1-PDGFR-induced myeloproliferative disease, Canc. Cell 3 (2003) 459–469.
[21] E. Leproult, S. Barluenga, D. Moras, J.M. Wurtz, N. Winssinger, Cysteine mapping in conformationally distinct kinase nucleotide binding sites: application to the design of selective covalent inhibitors, J. Med. Chem. 54 (2011) 1347–1355.
[22] C.H. Yun, T.J. Boggon, Y. Li, M.S. Woo, H. Greulich, M. Meyerson, M.J. Eck, Structures of lung cancer-derived EGFR mutants and inhibitor complexes: mechanism of activation and insights into differential inhibitor sensitivity, Canc. Cell 11 (2007) 217–227.
[23] W. Minor, M. Cymborowski, Z. Otwinowski, M. Chruszcz, HKL-3000: the integration of data reduction and structure solution–from diffraction images to an initial model in minutes, Acta. Crystallogr. D. Biol. Crystallogr 62 (2006) 859–866.
[24] A.J. McCoy, R.W. Grosse-Kunstleve, P.D. Adams, M.D. Winn, L.C. Storoni, R.J. Read, Phaser crystallographic software, J. Appl. Crystallogr. 40 (2007) 658–674.
[25] J. Griffith, J. Black, C. Faerman, L. Swenson, M. Wynn, F. Lu, J. Lippke, K. Saxena, The structural basis for autoinhibition of FLT3 by the juxtamembrane domain,

Mol. Cell. 13 (2004) 169–178.
[26] P. Emsley, K. Cowtan, Coot: model-building tools for molecular graphics, Acta. Crystallogr. D. Biol. Crystallogr 60 (2004) 2126–2132.
[27] P.D. Adams, P.V. Afonine, G. Bunkoczi, V.B. Chen, I.W. Davis, N. Echols, J.J. Headd, L.W. Hung, G.J. Kapral, R.W. Grosse-Kunstleve, A.J. McCoy, N.W. Moriarty, R. Oeffner, R.J. Read, D.C. Richardson, J.S. Richardson, T.C. Terwilliger, P.H. Zwart, PHENIX: a comprehensive Python-based system for macromolecular structure solution, Acta. Crystallogr. D. Biol. Crystallogr 66 (2010) 213–221.
[28] A. Sali, T.L. Blundell, Comparative protein modelling by satisfaction of spatial restraints, J. Mol. Biol. 234 (1993) 779–815.
[29] R.C. Edgar, MUSCLE: multiple sequence alignment with high accuracy and high throughput, Nucleic Acids Res. 32 (2004) 1792–1797.
[30] J.A. Bell, Y. Cao, J.R. Gunn, T. Day, E. Gallicchio, Z. Zhou, R. Levy, R. Farid, PrimeX and the Schrödinger computational chemistry suite of programs, Int. Tables. Crystallogr. (2012) 534–538.